Fast Global Oscillations in Networks of Integrate-and-Fire Neurons with Low Firing Rates

Nicolas Brunel
Vincent Hakim
LPS, Ecole Normale Supérieure, 75231 Paris Cedex 05, France

We study analytically the dynamics of a network of sparsely connected inhibitory integrate-and-fire neurons in a regime where individual neurons emit spikes irregularly and at a low rate. In the limit when the number of neurons $N \to \infty$, the network exhibits a sharp transition between a stationary and an oscillatory global activity regime where neurons are weakly synchronized. The activity becomes oscillatory when the inhibitory feedback is strong enough. The period of the global oscillation is found to be mainly controlled by synaptic times but depends also on the characteristics of the external input. In large but finite networks, the analysis shows that global oscillations of finite coherence time generically exist both above and below the critical inhibition threshold. Their characteristics are determined as functions of systems parameters in these two different regimes. The results are found to be in good agreement with numerical simulations.

1 Introduction

Oscillations are ubiquitous in neural systems and have been the focus of several recent studies (for reviews, see, e.g., Gray, 1994; Singer & Gray, 1995; Buzsáki & Chrobak, 1995; Ritz & Sejnowski, 1997). In particular, fast global oscillations in the gamma frequency range (> 30 Hz) have been reported in the visual cortex (Gray, König, Engel, & Singer, 1989; Eckhorn, Frien, Bauer, Woelbrun, & Kehr, 1993; Kreiter & Singer, 1996), in the olfactory cortex (Laurent & Davidowitz, 1994), and in the hippocampus (Bragin et al., 1995). Even faster oscillations (200 Hz) occur in the hippocampus of the rat (Buzsáki, Horvath, Urioste, Hetke, & Wise, 1992; Ylinen et al., 1995). In some experimental data (Eckhorn et al., 1993; Csicsvari, Hirase, Czurko, & Buzsáki, 1998; Fisahn, Pike, Buhl, & Paulsen, 1998) individual neuron recordings show irregular spike emission, at a rate that is low compared

to the global oscillation frequency.[1] This raises the question of whether a network composed of neurons firing irregularly at low rates can exhibit fast collective oscillations, which theoretical analyses and modeling studies may help to answer.

Previous studies of networks of spiking neurons have mostly analyzed, or simulated, synchronized oscillations in regimes in which neurons behave themselves as oscillators, with interspike intervals strongly peaked around their average value (Mirollo & Strogatz, 1990; Abbott & van Vreeswijk, 1993; van Vreeswijk, Abbott, & Ermentrout, 1994; Gerstner, 1995; Hansel, Mato, & Meunier, 1995; Gerstner, van Hemmen, & Cowan, 1996; Wang & Buzsáki, 1996; Traub, Whittington, Colling, Buzsáki, & Jefferys, 1996). Several oscillatory regimes have been found with either full or partial synchronization. A regime particular to globally coupled systems has been described where the network breaks into a few fully synchronized clusters (Golomb & Rinzel, 1994; van Vreeswijk, 1996). In some simulations of networks with detailed biophysical characteristics, cells fire sparsely and irregularly during a global oscillation (Traub, Miles, & Wong, 1989; Kopell & LeMasson, 1994; Wang, Golomb, & Rinzel, 1995), but the complexity of individual neurons in these models makes it difficult to understand the origin of the phenomenon clearly. The possible appearance of fast oscillations in a network where all neurons fire irregularly with an average frequency that is much lower than the population frequency therefore remains an intriguing question. It is the focus of the work presented here.

Recurrent inhibition plays an important role in the generation of synchronized oscillations as shown by in vivo (MacLeod & Laurent, 1996) and in vitro experiments (Whittington, Traub, & Jefferys, 1995) in different systems. This has been confirmed by several modeling studies (van Vreeswijk et al., 1994; Gerstner et al., 1996; Wang & Buzsáki, 1996; Traub et al., 1996). It has also been recently shown using simple models that networks in which inhibition balance excitation (Tsodyks & Sejnowski, 1995; Amit & Brunel, 1997a; van Vreeswijk & Sompolinsky, 1996) are naturally composed of neurons with low and irregular firing. Simulations (Amit & Brunel, 1997b) have shown that in one such model composed of sparsely connected integrate-and-fire (IF) neurons, the highly irregular single-neuron activity is accompanied by damped fast oscillations of the global activity.

In order to study the coexistence of individual neurons with low firing rates and fast collective oscillations in its simplest setting, we analyze in this article a sparsely connected network entirely composed of identical inhibitory IF neurons. Our aim is to provide a clear understanding of this

---

[1] Fast oscillations may be due in some cases to a synchronized subset of cells with high firing rates. The observation of cells with the required property has been recently reported in Gray & McCormick (1996).

type of synchrony and to determine:

- Under which conditions collective excitations of high frequencies arise in such networks

- What controls the different characteristics (amplitude, frequency, coherence time, . . .) of the global oscillation.

Simulation results, presented first, show that the essence of the phenomenon is present even in this simple system. Both neuron firing rates and the autocorrelation of the global activity are very similar to those reported in Amit and Brunel (1997b).

We begin by presenting simple arguments that give an estimation of the firing rate of individual neurons and the frequency of the global oscillation and that suggest that the global oscillation appears only above a well-defined parameter threshold.

In order to make the analysis more precise and complete, we then generalize the analytic approach of Amit and Brunel (1997a), which was restricted to the computation of firing rates in stationary states. The sparse random network connectivity leads the firing patterns of different neurons to be only weakly correlated. As a consequence, the network state can be described by the instantaneous distribution of membrane potentials of the neuronal population, together with the firing probability in this population. We obtain the coupled temporal evolution equations for these quantities, the time-independent solution of which coincides with the stationary solution of Amit and Brunel (1997a).

A linear stability analysis shows that this time-independent solution becomes unstable only when the strength of recurrent inhibition exceeds a critical level, in agreement with our simple arguments. When this critical level is reached, the stationary solution becomes unstable, and an oscillatory solution develops (via a Hopf bifurcation). The timescale of the period of the corresponding global oscillations is set by a synaptic time, independent of the firing rate of individual neurons, but the period precise value also depends on the characteristics of the external input.

The analysis is then pushed to higher orders. We obtain a reduced evolution equation describing the network collective dynamics. The effects coming from the finite size of the network are also discussed. We show that having a large but finite number of neurons gives a small stochastic component to the collective evolution equation. As a result, it is shown that cross-correlations in a finite network present damped oscillations both above and below the critical inhibition level. Below the critical level, the noise controls the oscillation amplitude, which decreases as the number of neurons is increased (at a fixed number of connections per neuron). Above the critical level, the main effect of the noise is to produce a phase diffusion of the global oscillation. An increase in the number of neurons results in an increase of
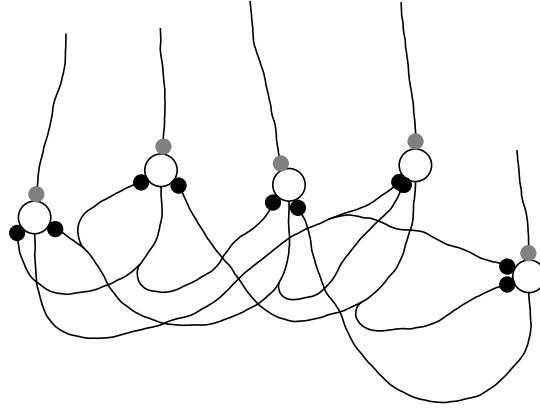
Figure 1: Schematic diagram of the connections in the network of N neurons. Each neuron (indicated as an open disk) receives C inhibitory connections (indicated as black) from within the network and C_{ext} excitatory connections (indicated as gray) from neurons outside the network.

the global oscillation coherence time and a reduced damping in average cross-correlations.

Finally, the effect of some of our simplifying assumptions is studied. We discuss the effect of allowing variability in synaptic times and number of synaptic connections from neuron to neuron. We also consider the effect of introducing a more detailed description of postsynaptic currents into the model. The technical aspects of our computations are detailed in the appendix.

2 Description of the Network and Simulations

We analyze the dynamics of a network composed of N identical inhibitory single compartment IF neurons. Each neuron receives C randomly chosen connections from other neurons in the network. It also receives C_{ext} connections from excitatory neurons outside the network (see Figure 1). We consider a sparsely connected case with $\epsilon = C/N \ll 1$.

Each neuron is simply described by its membrane potential. Let us suppose that neuron i receives an inhibitory (excitatory) connection from neuron j. When the presynaptic neuron j emits a spike at time t, the potential of the postsynaptic neuron i is decreased (increased) by J at time $t + \delta$ and returns exponentially to the resting potential in a time τ, which represents the integration time constant of the membrane. In this simple model, the single time δ is meant to represent the transmission delays but also, and most important, the longer time needed to obtain the full hyperpolariza-
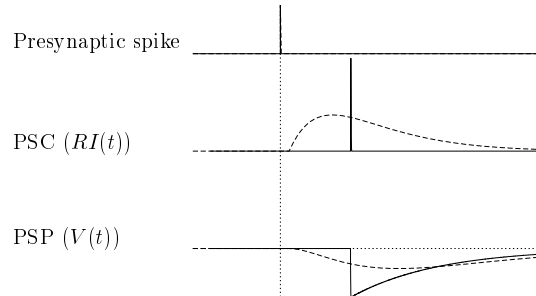
Figure 2: Comparison of the synaptic response characteristics in our model and in a more realistic model. (Top) The presynaptic spike. (Middle) The corresponding postsynaptic current (PSC). (Bottom) The corresponding postsynaptic potential (PSP) for a neuron initially at resting potential. Solid lines: Our model, in which the synaptic current is described by a delta function a time δ after the presynaptic spike. Dashed lines: A more realistic synaptic response, in which the PSC is described by an α-function with latency (transmission delay) τ_L and synaptic time constant τ_S $(t - \tau_L) \exp(-(t - \tau_L)/\tau_S)/\tau_S$. Our synaptic characteristic time δ can roughly be identified with the sum of latency and synaptic decay time, $\tau_L + \tau_S$. See the discussion in section 4.3.

tion of the postsynaptic neuron corresponding to a given presynaptic spike. Therefore, finding the correspondence between δ and the different synaptic timescales of a more realistic description needs some care. As pictorially shown in Figure 2, δ should roughly be identified to the characteristic duration of the synaptic currents. In the following, we thus refer to δ, which plays a crucial role in the generation of global oscillations, as the *synaptic time*. The correspondence between δ and the different synaptic timescales of a more realistic description is elaborated in section 4.3, where synaptic currents of finite duration are considered.

Mathematically, the depolarization $V_i(t)$ of neuron i $(i = 1, \ldots, N)$ at its soma obeys the equation,

$$\tau \dot{V}_i(t) = -V_i(t) + RI_i(t), \tag{2.1}$$

where $I_i(t)$ are the synaptic currents arriving at the soma. These synaptic currents are the sum of the contributions of spikes arriving at different synapses (both local and external). These spike contributions are modeled as delta functions in our basic IF model,

$$RI_i(t) = \tau \sum_j J_{ij} \sum_k \delta(t - t_j^k - \delta), \tag{2.2}$$

where the first sum on the right-hand side is a sum on different synapses ($j = 1, \ldots, C + C_{ext}$), with postsynaptic potential (PSP) amplitude (or efficacy) J_{ij}, while the second sum represents a sum on different spikes arriving at synapse j, at time $t = t_j^k + \delta$, where t_j^k is the emission time of kth spike at neuron j. For simplicity, we take PSP amplitudes equal at each synapse: $J_{ij} = J_{ext} > 0$ for excitatory synapses and $J_{ij} = -J$ for inhibitory ones. External synapses are activated by independent Poisson processes with rate ν_{ext}.

A firing threshold θ completes the description of the IF neuron. When $V_i(t)$ reaches θ, an action potential is emitted by neuron i, and the depolarization is reset to $V_r < \theta$ after a refractory period τ_{rp} during which the potential is insensitive to stimulation. A typical value would be $\tau_{rp} \sim 2$ ms. We are interested here in network states in which the frequency is much lower than the corresponding maximal frequency $1/\tau_{rp} \sim 500$ Hz. In this regime, we have checked that the exact value of τ_{rp} does not play any role. Thus, in the following we set τ_{rp} to zero for simplicity.

The outcome of a typical simulation is shown in Figure 3. Neurons are driven by the random external excitatory input above threshold; however, since feedback interactions are inhibitory, the global activity stays at rather low levels (about 5 Hz for the parameters indicated in Figure 3). For weak external noise levels ($\sigma_{ext} = 1$ mV), the global activity (total number of firing neurons in 0.4 ms bins) is strongly oscillatory with a period of about 7 ms, as testified by Figure 3C. On the other hand, increasing the external noise level strongly damps and decreases the amplitude of the global oscillation. Note that the global activity should roughly correspond to the local field potential (LFP) often recorded in neurophysiological experiments. On the other hand, even when the global activity is strongly oscillatory, individual firing is extremely irregular, as shown in the rasterfile of 50 neurons, Figure 3C (above the LFP), and in the ISI histogram (to the right of the spike rasters). In each oscillatory event, only a small fraction of the neurons fire.

This oscillatory collective behavior is also shown by fast oscillations in the temporal autocorrelation (AC) of the global activity, which are damped on a longer timescale (see Figure 3, to the right of the LFP). It is also reflected in the cross-correlations (CC) between the spike trains of a pair of neurons, which are typically equal to the AC of the global activity.

These simulation results raise several questions on the origin and characteristics of the observed oscillations. What is the mechanism of the fast oscillation? In which parameter region is the network oscillating? What are the network parameters that control the amplitude and the different timescales (frequency, damping time constant) of the global oscillation? How do they scale with the network size? The model is simple enough, and an analytical study gives precise answers to these questions, as shown in the following sections.
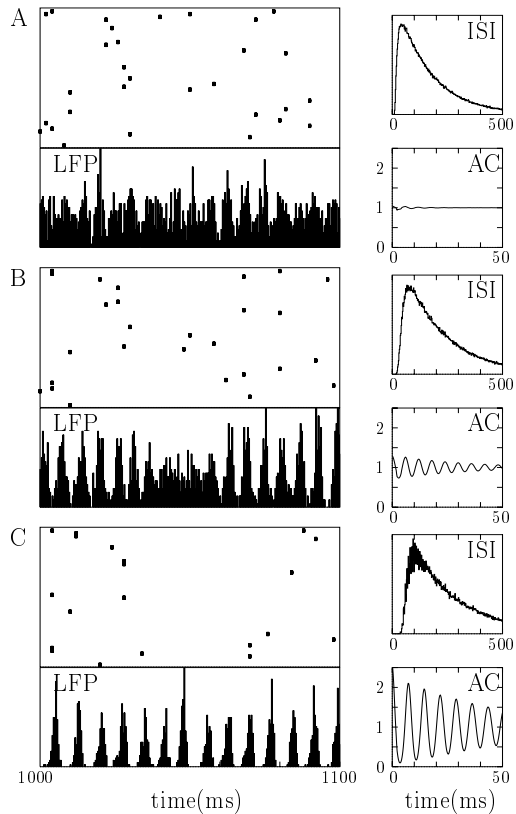
Figure 3: (Left) Time evolution of the global activity (LFP) during a 100 ms interval of the dynamics of a network of 5000 neurons (total number of firing neurons in 0.4 ms bins), together with spike rasters of 50 neurons, for different values of the external noise: $\sigma_{ext} = 5$ mV (A), 2.5 mV (B), and 1 mV (C). (Right) Autocorrelation of the global activity (AC) and interspike interval (ISI) histogram averaged over 1000 neurons, corresponding to the left pictures. Note the different timescales of AC and ISI in abscissa. Parameters: $\theta = 20$ mV, $V_r = 10$ mV, $\tau = 20$ ms, $\delta = 2$ ms, $C = 1000$, $J = 0.1$ mV, $\mu_{ext} = 25$ mV.

3 Analysis of the Network Dynamics

Several features simplify the analysis, as noted in a previous study (Amit & Brunel, 1997a) of the neuron mean firing rates. First, as a consequence of the network sparse random connectivity ($C \ll N$), two neurons share a small number of common inputs, and pair correlations can be neglected in the limit $C/N \to 0$. Second, we consider a regime where individual neurons

have a firing rate ν low compared to their inverse integration time $1/\tau$ and receive a large number of inputs per integration time τ, each input making a small contribution compared to the firing threshold ($J \ll \theta$).[2] In this situation, the synaptic current of a neuron can be approximated by an average part plus a fluctuating gaussian part, and the spike trains of all neurons in the network can be self-consistently described by Poisson processes with a common instantaneous firing rate $\nu(t)$ but otherwise uncorrelated from neuron to neuron (that is, between t and $t+dt$, a spike emission has a probability $\nu(t)dt$ of occurring for each neuron, but these events occur statistically independently in different neurons).

The synaptic current at the soma of a neuron (neuron i) can thus be written as

$$RI_i(t) = \mu(t) + \sigma\sqrt{\tau}\eta_i(t). \tag{3.1}$$

The average part $\mu(t)$ is related to the firing rate at time $t - \delta$ and is a sum of local and external inputs:

$$\mu = \mu_l + \mu_{ext} \ \text{ with } \ \mu_l = -CJ\nu(t-\delta)\tau, \quad \mu_{ext} = C_{ext}J_{ext}\nu_{ext}\tau. \tag{3.2}$$

Similarly the fluctuating part, $\sigma\sqrt{\tau}\eta_i(t)$, is given by the fluctuation in the sum of internal and external Poissonian inputs of rate $C\nu$ and $C_{ext}\nu_{ext}$. Its magnitude is given by

$$\sigma^2 = \sigma_l^2 + \sigma_{ext}^2 \ \text{ with } \ \sigma_l = J\sqrt{C\nu(t-\delta)\tau}, \quad \sigma_{ext} = J_{ext}\sqrt{C_{ext}\nu_{ext}\tau}, \tag{3.3}$$

and $\eta_i(t)$ is a gaussian white noise uncorrelated from neuron to neuron, $\langle\eta_i(t)\rangle = 0$ and $\langle\eta_i(t)\eta_j(t')\rangle = \delta_{i,j}\delta(t - t')$.

Before describing our precise results, it may be useful to give simple estimates that show how the neuron firing rates, the collective oscillation frequency, and the oscillatory threshold can be obtained from equations 3.1–3.3.

Let us first consider the stationary case. The case of interest corresponds to $\mu < \theta$. When expression 3.1 is used for the synaptic current, the dynamics of the neuron depolarization (see equation 2.1) is a stochastic motion in the harmonic potential $(V - \mu)^2$ truncated at the firing threshold $V = \theta$. The neuron firing rate ν_0 is the escape rate from this potential. For a weak noise, it is given by the inverse of the timescale of the motion $1/\tau$ diminished by an Arrhenius activation factor. So one obtains the simple estimate (up to an algebraic prefactor),

$$\nu_0 \sim \frac{1}{\tau}\exp\left(-\frac{(\theta - \mu)^2}{\sigma^2}\right). \tag{3.4}$$

---

[2] Typical numbers in cortex are $C = 5000$, $\tau = 20$ ms, $\nu = 5$ Hz, $J = 0.1$ mV, $\theta = 20$ mV so that $C\nu\tau$ is typically several hundreds while θ/J is of order 100 (Abeles, 1991; Braitenberg & Shütz, 1991). In the simulation shown in Figure 3 $C\nu\tau \sim 100$, $\theta/J \sim 200$.

This becomes a self-consistent equation for v_0 once μ and σ are expressed in terms of v_0 using equations 3.2 and 3.3. The simple estimate, equation 3.4, is made precise below by following Kramers's classic treatment of the thermal escape over a potential barrier (Chandrasekhar, 1943).

The origin of the collective oscillation can also be simply understood. An increase of activity in the network due to a fluctuation provokes an increase in the average feedback inhibitory input. Thus, after a period of about one synaptic time, the activity should decrease due to the increase of the inhibitory input. This decrease will itself provoke a decrease in the inhibitory input and a corresponding increase in the activity after a new period equal to the synaptic time. This simple argument predicts a global oscillation period of about a couple of times the synaptic time δ—not too far from the period observed in the simulations. However, it does not seem to have been noted previously that a global oscillation of period δ can in fact occur only if it is not masked by the intrinsic noise in the system. The resulting oscillation threshold can be simply estimated in the limit where δ is short compared to the timescale of the depolarization dynamics. During a short time interval δ, a neuron membrane potential receives from the local network an average input of magnitude $Cv_0\delta J$. The fluctuation in its membrane potential in the same time interval (due to intrinsic fluctuations in the total incoming current) is $\sigma\sqrt{\delta/\tau}$. The change in the average local input can be detected only if it is larger than the intrinsic potential fluctuations. A global oscillation can therefore occur only when

$$\frac{CJv_0\tau}{\sigma} = -\frac{\mu_l}{\sigma} \gtrsim \sqrt{\frac{\tau}{\delta}}.$$

These simple estimations are confirmed by the analysis presented below and replaced by precise formulas.

3.1 Dynamics of the Distribution of Neuron Potentials. When pair correlations are neglected, the system can be described by the distribution of the neuron depolarization $P(V, t)$—that is, the probability of finding the depolarization of a randomly chosen neuron at V at time t. This distribution is the (normalized) histogram of the depolarization of all neurons at time t in the large N limit $N \to \infty$. The stochastic equations, 2.1 and 3.1 for the dynamics of a neuron depolarization can be transformed into a Fokker-Planck equation describing the evolution of their probability distribution (Chandrasekhar, 1943),

$$\tau\frac{\partial P(V, t)}{\partial t} = \frac{\sigma^2(t)}{2}\frac{\partial^2 P(V, t)}{\partial V^2} + \frac{\partial}{\partial V}\left[(V - \mu(t))P(V, t)\right]. \tag{3.5}$$

The two terms on the r.h.s. of equation 3.5 correspond respectively to a diffusion term coming from the current fluctuations and a drift term coming from the average part of the synaptic input. $\sigma(t)$ and $\mu(t)$ are related to

$v(t - \delta)$, the probability per unit time of spike emission at time $t - \delta$, by equations 3.2 and 3.3. Note that the Fokker-Planck equation has been used previously in studies of globally coupled oscillators (Sakaguchi, Shinomoto, & Kuramoto, 1988; Strogatz & Mirollo, 1991; Abbott & van Vreeswijk, 1993; Treves, 1993).

The resetting of the potential at the firing threshold ($V = \theta$) imposes the absorbing boundary condition $P(\theta, t) = 0$. Moreover, the probability current through θ gives the probability of spike emission at t,

$$\frac{\partial P}{\partial V}(\theta, t) = -\frac{2\nu(t)\tau}{\sigma^2(t)}. \tag{3.6}$$

At the reset potential $V = V_r$, $P(V, t)$ is continuous, but the entering probability current imposes the following derivative discontinuity:

$$\frac{\partial P}{\partial V}(V_r^+, t) - \frac{\partial P}{\partial V}(V_r^-, t) = -\frac{2\nu(t)\tau}{\sigma^2(t)}. \tag{3.7}$$

At $V = -\infty$, P should tend sufficiently quickly toward zero to be integrable, that is,

$$\lim_{V \to -\infty} P(V, t) = 0 \quad \lim_{V \to -\infty} VP(V, t) = 0. \tag{3.8}$$

Last, $P(V, t)$ is a probability distribution and should satisfy the normalization condition:

$$\int_{-\infty}^{\theta} P(V, t)dV = 1. \tag{3.9}$$

3.2 Stationary States. We first consider stationary solutions $P(V, t) = P_0(V)$. Time-independent solutions of equation 3.5 satisfying the boundary conditions—equations 3.6–3.8—are given by

$$P_0(V) = 2\frac{\nu_0\tau}{\sigma_0} \exp\left(-\frac{(V - \mu_0)^2}{\sigma_0^2}\right) \int_{\frac{V-\mu_0}{\sigma_0}}^{\frac{\theta-\mu_0}{\sigma_0}} \Theta\left(u - \frac{V_r - \mu_0}{\sigma_0}\right) e^{u^2} du, \tag{3.10}$$

with

$$\mu_0 = -CJ\nu_0\tau + \mu_{ext}, \quad \sigma_0^2 = CJ^2\nu_0\tau + \sigma_{ext}^2 \tag{3.11}$$

(in equation 3.10, $\Theta(x)$ denotes the Heaviside function, $\Theta(x) = 1$ for $x > 0$ and $\Theta(x) = 0$ otherwise). The normalization condition, equation 3.9, provides the self-consistent condition that determines ν_0:

$$\frac{1}{\nu_0\tau} = 2\int_{\frac{V_r-\mu_0}{\sigma_0}}^{\frac{\theta-\mu_0}{\sigma_0}} due^{u^2} \int_{-\infty}^{u} dve^{-v^2}$$

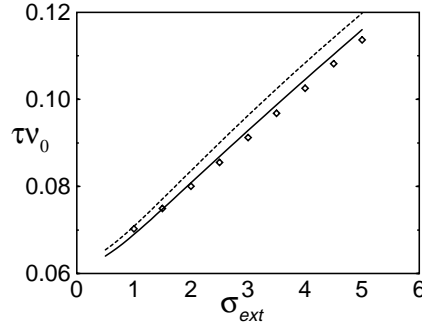$$= \int_0^{+\infty} due^{-u^2}\left[\frac{e^{2y_\theta u} - e^{2y_r u}}{u}\right], \tag{3.12}$$

Figure 4: Neuron firing rate versus σ_{ext}: simulation ($\diamond$); solution of equation 3.12 (solid line); solution of the approximate asymptotic form, equation 3.13 (dashed line). Others parameters are fixed as in Figure 2: $\tau = 20$ ms, $J = 0.1$ mV, $C = 1000$, $N = 5000$, $\theta = 20$ mV, $V_r = 10$ mV, $\mu_{ext} = 25$ mV, $\delta = 2$ ms.

with $y_\theta = \frac{\theta - \mu_0}{\sigma_0}$, $y_r = \frac{V_r - \mu_0}{\sigma_0}$. In the regime $(\theta - \mu_0) \gg \sigma_0$, equation 3.12 becomes

$$\nu_0 \tau \simeq \frac{(\theta - \mu_0)}{\sigma_0 \sqrt{\pi}} \exp\left(-\frac{(\theta - \mu_0)^2}{\sigma_0^2}\right). \tag{3.13}$$

In Figure 4, the firing rates obtained by solving equations 3.12 and 3.13 are compared with those obtained from simulations of the network. It shows an almost linear increase in the rates as a function of σ_{ext} in the range 3–6 Hz and a good agreement between equation 3.12 and the results of simulations. The asymptotic expression, equation 3.13, is also rather close to the simulation results in this range of σ.

3.3 Linear Stability of the Stationary States. We can now investigate in which parameter regime the time-independent solution $(P_0(V), \nu_0)$ is stable. To simplify the study of the Fokker-Planck equation, 3.5, it is convenient to rescale P, V, and ν by

$$P = \frac{2\tau\nu_0}{\sigma_0}Q, \quad y = \frac{V - \mu_0}{\sigma_0}, \quad \nu = \nu_0(1 + n(t)). \tag{3.14}$$

y is the difference between the membrane potential and the average input in the stationary state, in units of the average fluctuation of the input in the stationary state. $n(t)$ corresponds to the relative variation of the instantaneous frequency around the stationary frequency. After these rescalings, equation 3.5 becomes

$$\tau \frac{\partial Q}{\partial t} = \frac{1}{2} \frac{\partial^2 Q}{\partial y^2} + \frac{\partial}{\partial y}(yQ) + n(t - \delta)\left(G \frac{\partial Q}{\partial y} + \frac{H}{2} \frac{\partial^2 Q}{\partial y^2}\right), \tag{3.15}$$

where G is the ratio between the mean local inhibitory inputs and σ_0, and H is the ratio between the variance of the local inputs and the total variance (local plus external):

$$G = \frac{CJ\tau\nu_0}{\sigma_0} = \frac{-\mu_{0,l}}{\sigma_0}, \quad H = \frac{CJ^2\tau\nu_0}{\sigma_0^2} = \frac{\sigma_{0,l}^2}{\sigma_0^2}. \tag{3.16}$$

These parameters are a measure of the relative strength of the recurrent inhibitory interactions.

Equation 3.15 holds on the two intervals: $-\infty < y < y_r$ and $y_r < y < y_\theta$. The boundary conditions on Q are imposed at $y_\theta = \frac{\theta - \mu_0}{\sigma_0}$ and $y_r = \frac{V_r - \mu_0}{\sigma_0}$. Those on the derivatives of Q read

$$\frac{\partial Q}{\partial y}(y_\theta, t) = \frac{\partial Q}{\partial y}(y_r^+, t) - \frac{\partial Q}{\partial y}(y_r^-, t) = -\frac{1 + n(t)}{1 + Hn(t - \delta)}. \tag{3.17}$$

The linear stability of the stationary solution is studied in detail Section A.1. This can be done in a standard way (Hirsch & Smale, 1974) by expanding $Q = Q_0 + Q_1 + \cdots$ and $n = n_1 + \cdots$ around the steady-state solution. The linear equation obtained at first order has solutions that are exponential in time, $Q_1 = \exp(wt/\tau)\hat{Q}_1$, $n_1 \sim \exp(w/\tau)\hat{n}_1$, where w is a solution of the eigenvalue equation, A.29 of the appendix. The stationary solution becomes unstable when the real part of w becomes positive.

When the synaptic time δ becomes much smaller than τ, the roots w of this equation become large. We consider the regime $\delta/\tau \ll 1$ but $\delta/\tau \gg 1/C$, which is the relevant case in simulations and corresponds to the realistic regime. $\delta/\tau \gg 1/C$ is needed because otherwise the equations giving G and H become inconsistent with the condition $\tau\nu_0 \ll 1$. At the oscillatory instability onset, w is purely imaginary $w = i\omega_c$, where ω_c/τ is the frequency of the oscillation that develops. The eigenvalue equation takes in the limit $\delta/\tau \to 0$, $\omega \to \infty$ the form

$$\left[\frac{G}{\sqrt{\omega_c}}(i - 1) + H\right]\exp(-i\omega_c\delta/\tau) = 1. \tag{3.18}$$

In this limit, the instability line in the parameter space (G, H) is obtained parametrically as

$$G = \sqrt{\omega_c}\sin\left(\frac{\omega_c\delta}{\tau}\right)$$

$$H = \sin\left(\frac{\omega_c\delta}{\tau}\right) + \cos\left(\frac{\omega_c\delta}{\tau}\right).$$

H is by definition constrained to be between 0 and 1 (it is the ratio between local and total variances): $H = 0$ corresponds to the limit of very large

external fluctuations, $\sigma_{ext} \gg \sigma_l$, while $H = 1$ corresponds to $\sigma_{ext} = 0$. We find that the frequency of the oscillation varies from

$$\frac{\omega_c}{\tau} = \frac{3\pi}{4\delta} \quad \text{when } H = 0, \text{ to}$$

$$\frac{\omega_c}{\tau} = \frac{\pi}{2\delta} \quad \text{when } H = 1. \tag{3.19}$$

This corresponds to an oscillation with a period between $8\delta/3$ and 4δ, not too far from the value 2δ obtained by simple arguments. At the same time the critical value of G goes from

$$G_c = \sqrt{\frac{3\pi\tau}{8\delta}} \quad \text{when } H = 0, \text{ to}$$

$$G_c = \sqrt{\frac{\pi\tau}{2\delta}} \quad \text{when } H = 1.$$

The oscillation threshold G_c is proportional to $\sqrt{\tau/\delta}$ as anticipated.

   This instability line can be translated in terms of the parameters μ_{ext}, σ_{ext}, and calculated numerically using equation A.29 for any value of the network parameters. This line of instability in the plane $(\mu_{ext}, \sigma_{ext})$ is shown in the right part of Figure 5. The stationary solution is unstable above the solid line. Thus, if the external input is Poissonian, an increase in the frequency of external stimulation will typically bring the network from the stationary to the oscillatory regime, as indicated by the dashed line in Figure 5, which represents the average (μ_{ext}) and the fluctuations (σ_{ext}) of the external inputs when the frequency of a Poissonian external input through synapses of strength $J_{ext} = 0.1$ mV is varied.

   3.4 Weakly Nonlinear Analysis. The linear stability analysis of the previous section shows that a small oscillation grows when one crosses the instability line in the plane μ_{ext}, σ_{ext}. But it does not say much on the characteristics of the resulting finite amplitude oscillation. In order to describe it and to be able to compare quantitatively analytic results to simulation data, one needs to compute the nonlinear terms that saturate the instability growth. This can be done in a standard manner (Bender & Orszag, 1987) by computing terms beyond the linear order in an expansion around the stationary state. The explicit computation is detailed in Section A.2. The collective oscillation is determined by the deviation n_1 of the neuron firing rate from its stationary value:

$$n_1(t) = \hat{n}_1(t) \exp(i\omega_c t/\tau) + \hat{n}_1^\star(t) \exp(-i\omega_c t/\tau).$$

$\hat{n}_1$ determines the amplitude of the collective oscillation as well as the nonlinear contribution to its frequency in the vicinity of the instability line.
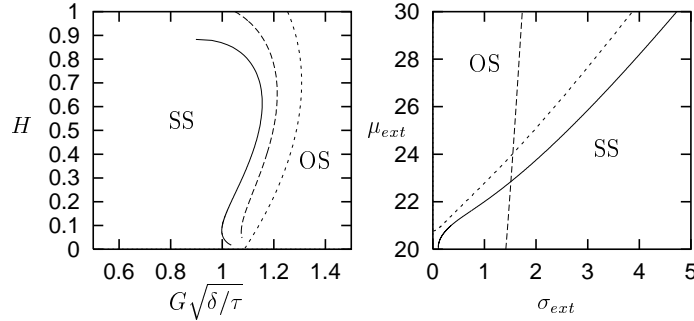
Figure 5: (Left) Instability line in the plane (H, $G\sqrt{\delta/\tau}$). Solid line: Instability line for parameters of Figure 3 and $\delta = 0.1\tau$. Long-dashed line: $\delta = 0.05\tau$. Short-dashed line: asymptotic limit $\delta/\tau \to 0$. The stationary state (SS) is unstable to the right of the instability line, where an oscillatory instability (OS) develops. (Right) Instability line in the plane (μ_{ext}, σ_{ext}). Solid line: Parameters of Figure 2, and $\delta = 0.1\tau$. The short-dashed line is constructed taking the asymptotic instability line in the plane (H, $G\sqrt{\delta/\tau}$) and calculating the corresponding instability line in (μ_{ext}, σ_{ext}) with $\delta = 0.1\tau$. The SS becomes unstable above the instability line. The long-dashed line shows the average (μ_{ext}) and the fluctuations (σ_{ext}) of the external inputs when the frequency of a Poissonian external input through synapses of strength $J_{ext} = 0.1$ mV is varied. For low external frequencies, the network is in its stationary state. When the external frequency increases, the network goes to OS.

The analysis shows that the dynamics of the (small) deviation around the stationary firing rate can be described by the reduced equation,

$$\tau \frac{d\hat{n}_1}{dt} = A\hat{n}_1 - B|\hat{n}_1|^2\hat{n}_1, \tag{3.20}$$

in which A and B are complex numbers. The value of A comes from the linear stability analysis. If $\text{Re}(A) < 0$ a small initial value of n_1 decays, and the stationary state is stable. On the contrary, if $Re(A) > 0$, a global oscillation develops. When $|\hat{n}_1|$ grows, the second nonlinear term on the r.h.s. of equation 3.20 becomes important. It is found here that $\text{Re}(B) > 0$ (a "normal" or "supercritical" Hopf bifurcation) so that the nonlinear term saturates the linear growth. The characteristics of the oscillatory final state come from the balance between the two terms.

The explicit expression of A and B is given in equations A.54 and A.55 as a ratio of hypergeometric functions of the network parameters. A depends linearly on the deviation of the parameters G and H from their critical values, that is, $G - G_c$, $H - H_c$. In the limit $\delta/\tau \to 0$, the expressions of A and B simplify. For example, when $H = 0$ (large external fluctuations), we find in

the limit $\delta/\tau \to 0$

$$A = \frac{\tau}{\delta} \frac{(1+2i/3\pi)}{(1+4/9\pi^2)} \frac{G-G_c}{G_c} \simeq \frac{\tau}{\delta} (1.35 + 0.29i) \frac{G-G_c}{G_c}$$

$$B = \frac{\tau}{\delta} \left(\frac{9\pi^2}{4+9\pi^2} \right) \left[\frac{13-5\sqrt{2}}{10} - \frac{9-5\sqrt{2}}{15\pi} + i \left(\frac{13-5\sqrt{2}}{15\pi} + \frac{9-5\sqrt{2}}{10} \right) \right]$$

$$\simeq \frac{\tau}{\delta}(0.53 + 0.30i). \tag{3.21}$$

Generally the complex numbers A and B can be written in terms of their real and imaginary parts, $A = A_r + iA_i$, $B = B_r + iB_i$. On the critical line, that is, for $G = G_c$, $H = H_c$, $A_r = A_i = 0$; above the critical line an instability develops, $A_r > 0$, proportionally to $G - G_c$ and $H - H_c$. The amplitude of this instability is controlled by the cubic term. The stable limit cycle solution of equation 3.20, above the critical line, is

$$\hat{n}_1(t) = R \exp\left(i\Delta\omega \frac{t}{\tau} \right), \tag{3.22}$$

where

$$R = \sqrt{\frac{A_r}{B_r}} \quad \text{and} \quad \Delta\omega = A_i - B_i \frac{A_r}{B_r}.$$

The autocorrelation (AC) of the global activity, normalized by ν_0, is, when $A_r > 0$,

$$C(s) = \lim_{T \to \infty} \frac{1}{T-s} \int_0^{T-s} (1 + n_1(t))(1 + n_1(t+s)) dt \tag{3.23}$$

$$= 1 + 2R^2 \cos\left[(\omega_c + \Delta\omega)s/\tau \right].$$

The AC is a cosine function of frequency $(\omega_c + \Delta\omega)/\tau$ and amplitude R^2. Compared with the AC function observed in the simulation, Figure 3C, we see a qualitative difference: there is no damping of the oscillation. The next section shows that the damping is due to finite size effects. We analyze them before comparing quantitatively the analytical results with simulations.

3.5 Finite Size Effects and Phase Diffusion of the Collective Oscillation. We discuss the effect of having a large but finite number of neurons in the network. It is well known that for stochastic dynamics, a sharp transition can occur only in the limit $N \to \infty$ and that it will be smoothed by finite size effects. In the sparse connectivity limit, which allows treating the quenched

random geometry of the lattice in an annealed fashion,[3] the fluctuations in the input of a given neuron i can be seen as the result of the randomness of two different processes. The first is the spike emission process $S(t)$ of the whole network, and the second, for each spike emitted by the network, is the presence or absence of a synapse between the neuron that emitted the spike and the considered neuron. If a spike is emitted at time t, $\rho_i(t) = 1$ with probability C/N, and 0 otherwise. The input to the network is then

$$RI_i(t) = -J\tau\rho_i(t)S(t - \delta).$$

Both processes can be decomposed between their mean and their fluctuation,

$$\rho_i(t) = \frac{C}{N} + \delta\rho_i(t), \quad S(t) = N\nu(t) + \delta S(t).$$

Thus the input becomes

$$RI_i(t) = \mu(t) - J\tau N\nu(t)\delta\rho_i(t) - J\tau\frac{C}{N}\delta S(t),$$

in which $\mu(t)$ is given by equation 3.20. The input is the sum of a constant part μ and of two distinct random processes superimposed on μ. The first is uncorrelated from neuron to neuron, and we have already seen in section 3 that it can be described by N uncorrelated gaussian white noises $\sigma\sqrt{\tau}\eta_i(t)$, $i = 1, \ldots, N$ where $\langle\eta_i(t)\eta_j(t')\rangle = \delta_{ij}\delta(t - t')$. The second part is independent of i. It comes from the intrinsic fluctuations in the spike train of the whole network that are seen by all neurons. This part becomes negligible when $\epsilon = C/N \to 0$, but can play a role, as we will see, when C/N is finite. The global activity in the network is essentially a Poisson process with instantaneous frequency $N\nu(t)$. Such a Poisson process has mean $N\nu(t)$, which is taken into account in μ, and variance $N\nu(t)\delta(t - t')$. The fluctuating part of this process is well approximated by a gaussian white noise $\sqrt{N\nu_0}\xi(t)$, where ($\xi(t)$ satisfies $\langle\xi(t)\rangle = 0$, $\langle\xi(t)\xi(t')\rangle = \delta(t - t')$). Note that for simplicity we take the variance of this noise to be independent of time, which is the case for $n_1(t) \ll 1$. These fluctuations are global and perceived by all neurons in the network. Thus, the mean synaptic input received by the neurons becomes

$$CJ\tau\nu(t) + J\sqrt{\epsilon C\nu_0\tau}\sqrt{\tau}\xi(t) + \mu_{ext}.$$

Inserting this mean synaptic input in the drift term of the Fokker-Planck equation, we can rewrite equation 3.15 as

$$\tau\frac{\partial Q}{\partial t} = \frac{\partial}{\partial y}\{[y + Gn(t - \delta) + \eta\sqrt{\tau}\xi(t)]Q\} + \frac{1}{2}\frac{\partial^2 Q}{\partial y^2}, \tag{3.24}$$

---

[3] Here we do not consider the correlations due to the quenched connectivity for finite ϵ. These correlations would give small corrections to the parameters calculated in the limit $\epsilon \to 0$, but do not give rise to qualitatively new effects for the global activity such as the phase diffusion phenomenon discussed in this section.

where η denotes the intensity of the noise stemming from these global fluctuations. η tends to zero as the network size increases

$$\eta = \sqrt{\epsilon}\frac{\sigma_0^l}{\sigma_0}. \tag{3.25}$$

Taking into account this global noise term in the derivation of the reduced equation, we obtain,

$$\tau\frac{d\hat{n}_1}{dt} = A\hat{n}_1 - B|\hat{n}_1|^2\hat{n}_1 + D\sqrt{\tau}\zeta(t) \tag{3.26}$$

in which A, B, and D are given by Equations A.54, A.55, and A.57, and ζ is a complex white noise such that $\langle\zeta(t)\zeta^\star(t')\rangle = \delta(t - t')$. D is proportional to η—to both the square root of the connection probability and the ratio between local and total fluctuations.

Thus, the effect of the finite size of the network is to add a small stochastic component to the evolution equation of n_1, equation 3.26. Its main effect is to produce a phase diffusion of the collective oscillation, which leads to the damping of the oscillation in the autocorrelation function (for a similar effect in a simple model see also Rappel & Karma, 1996).

3.5.1 Amplitude of the Autocorrelation. From the reduced equation 3.26, one can compute exactly the autocorrelation at zero time $C(0)$ as shown in the appendix. This gives:

- In the stationary regime far from the critical line, $A_r < 0$, $|D|/|A_r| \ll 1$:

$$C(0) - 1 \sim \frac{|D|^2}{|A_r|} \sim O\left(\frac{C}{N}\right). \tag{3.27}$$

  The amplitude of the fluctuations in the global activity is proportional to C/N and thus vanishes when the connection probability goes to zero.

- On the critical line, $A_r = 0$:

$$C(0) - 1 = \frac{2|D|}{\sqrt{\pi B_r}} \sim O\left(\sqrt{\frac{C}{N}}\right). \tag{3.28}$$

  The amplitude of the fluctuations is proportional to the square root of the connection probability.

- In the oscillatory regime far from the critical line, $A_r > 0$, $|D|/A_r \ll 1$:

$$C(0) - 1 \sim \frac{2A_r}{B_r} \sim O(1). \tag{3.29}$$

  In this regime the amplitude of the oscillation is to leading order independent of the noise amplitude.

3.5.2 Oscillations Below the Critical Line. In the stationary regime far from the critical line, the fluctuations of activity n_1 provoked by the noise term can be considered small, and thus we can neglect the cubic term. It is then easy to calculate the autocorrelation (AC) of the activity,

$$C(s) = 1 + \frac{|D|^2}{|A_r|} \exp\left(-\frac{|A_r|s}{\tau}\right) \cos\left([\omega_c + A_i]\frac{s}{\tau}\right). \tag{3.30}$$

It is a damped cosine function. The damped oscillation has frequency $(\omega_c + A_i)/\tau$ and damping time constant proportional to $\tau/|A_r|$. The amplitude of the autocorrelation function is proportional to C/N.

3.5.3 Oscillations Above the Critical Line. In the oscillatory regime far from the critical line, we find in Section A.3 an AC function of the form

$$C(s) = 1 + 2\frac{A_r}{B_r} \cos\left((\omega_c + \Delta\omega)s/\tau\right) \exp\left(-\frac{\gamma^2(s)}{2}\right). \tag{3.31}$$

It is again a damped cosine function. The damping factor $\exp(-\gamma^2(s)/2)$ is different from an exponential only at short times $s \sim \delta$. At longer times, $s \gg \delta$, we obtain again an exponential

$$\exp\left(-\frac{\gamma^2(s)}{2}\right) = \exp\left(-\frac{|D|^2}{4R^2}\left(1 + \frac{B_i^2}{B_r^2}\right)\frac{s}{\tau}\left[1 + \frac{|D|^2}{2A_r} + O\left(|D|^4\right)\right]\right).$$

The damping time constant is proportional to leading order in $|D|$ to $1/|D|^2 \sim N/C$, that is, to the inverse of the connection probability. When N goes to infinity at C fixed, the "coherence time" of the oscillation increases linearly with N.

This "phase diffusion" effect is the main finite size effect above the critical line. Both the amplitude and frequency of the oscillation are essentially unaffected by these finite size effects.

3.6 Comparison Between Simulations and Theory. The autocorrelation (AC) of the global activity was computed for each set of parameters from a simulation of 20 seconds. A few longer simulations were performed as a check. The autocorrelations obtained in the longer simulations are essentially identical to the one obtained in the 20 s simulation.

Since the analysis predicts AC functions described by damped cosine functions, a least-square fit of all AC functions was performed with such functions. Thus the full AC is reduced to three parameters: its amplitude at zero lag C_0, its frequency ω, and its damping time constant (or coherence time) τ_c,

$$C(s) = 1 + C_0 \exp\left(-\frac{|s|}{\tau_c}\right) \cos(\omega s).$$

We then compared the result of the fitting procedure with the analytical expressions.

We varied the magnitude of the external noise σ_{ext} from 0 to 5 mV. This brings the network from the oscillatory to the stationary state.

In Figure 6 we plot the results of simulations and theory. In these figures the diamonds are the simulation results and the dashed lines the analytical results. In Figure 6A, the short-dashed line indicates the amplitude in the limit $N \to \infty$, while the long-dashed line indicates the amplitude calculated analytically taking into account finite size effects. The crosses are obtained simulating numerically the reduced equation, equation 3.26. We find that in the stationary regime as well as in the oscillatory regime close to the bifurcation point, the amplitude of the oscillation obtained in the simulation is in very good agreement with the calculation (see Figure 6A). On the other hand, as the amplitude of the oscillation becomes of the same order as the average frequency, $C_0 \sim 1$, higher-order effects become important and the calculation overestimates the amplitude of the AC. For the frequency of the oscillation (see Figure 6B), the calculation reproduces quite well the results of the simulations, except for very low noise levels, for which we are rather far from the bifurcation point. Note that the frequency ranges for this set of parameters from 70 to 180 Hz, depending on the level of external noise. Thus, without varying the time constants τ and δ, we find that the same network is able to sustain a collective oscillation at quite different frequencies.

Finally, the approximate analytical expressions for the damping time constant agree well with the simulation away from the bifurcation point, as expected (see Figure 6C). On the other hand, the simulation of the reduced equation is in good agreement with the network simulations in the whole range of σ_{ext}.

In Figure 7 we compare the full AC functions from theory (simulation of the reduced equation) and network simulations in three regimes to show the good agreement between both.

4 Extensions

In the previous sections a very simple network has been analyzed, and the question of the effect of some of our simplifying assumptions legitimately arises. In particular, we have chosen exactly identical neurons. It can be wondered how the results are modified when some variations in neuron properties are taken into account. In order to address this question, we show how the previous analysis can be generalized in two cases. Since we have seen that the oscillation frequency is tightly linked to synaptic times, the effect of a fluctuation in synaptic times is investigated first. We then consider the effect of a fluctuation in the number of connections per neuron, which has been found to result in a wide spectrum of neuron steady discharge rates (Amit & Brunel, 1997b). In both cases, it is reassuring to find that the picture obtained from the simple model analysis remains accurate. We
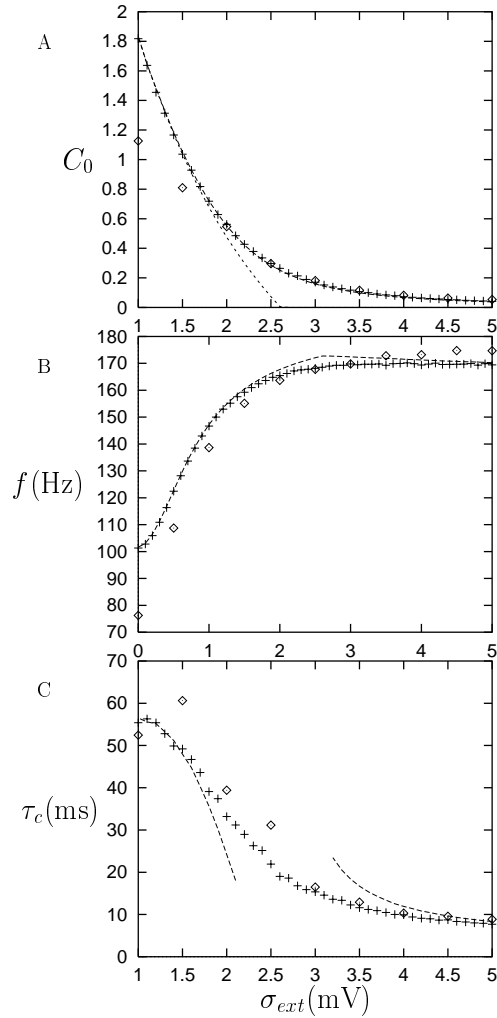
Figure 6: Parameters of the AC function versus σ_{ext}. (A) Amplitude of the AC at zero lag. (B) Frequency. (C) Damping time constant. Diamonds: Simulation of the full network. Crosses: Simulation of the reduced equation. Dashed lines: Theory. In (A), the short-dashed line represents the amplitude in the limit $N \rightarrow \infty$ Parameters: $\tau = 20$ ms, $J = -0.1$ mV, $C = 1000$, $N = 5000$, $\theta = 20$ mV, $V_r = 10$ mV, $\mu_{ext} = 25$ mV, $\delta = 2$ ms.

finally consider a model with synaptic currents of finite duration to analyze more precisely which timescale plays the role of our "synaptic time" in this more realistic case.
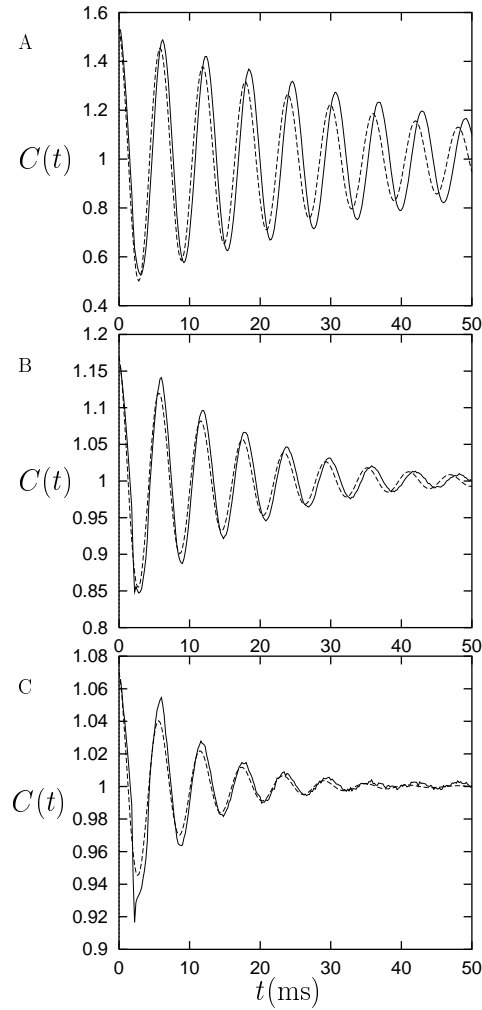
Figure 7: Autocorrelations. (A) $\sigma_{ext} = 2$ mV. (B) $\sigma_{ext} = 3$ mV. (C) $\sigma_{ext} = 4$ mV. Parameters as in Figure 6. Solid lines: Network simulation. Dashed lines: Theory (simulation of the reduced equation).

4.1 Effect of Inhomogeneous Synaptic Times. The analysis can easily be extended to the case in which time constants at each synaptic site are drawn randomly and independently from an arbitrary probability density function (PDF) $\Pr(\delta)$ (see Section A.4). In the following we consider the case of a uniform PDF between 0 and 2δ.
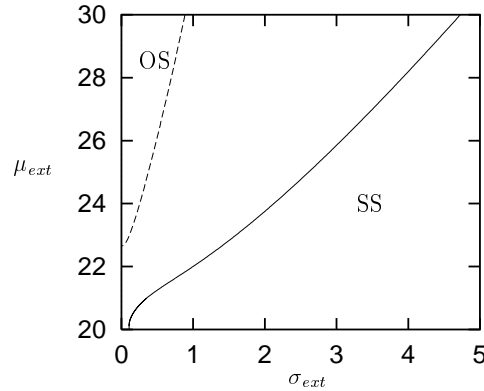
Figure 8: Instability line in the plane $(\mu_{ext}, \sigma_{ext})$ for $\tau = 20$ ms, $J = 0.1$ mV, $C = 1000$, $\theta = 20$ mV, $V_r = 10$ mV, $\delta = 2$ ms. Solid line: All synaptic times equal to δ. Dashed line: Synaptic times drawn from a uniform distribution from 0 to 2δ.

Figure 8 shows how the instability line is modified by random synaptic times. The region where the oscillatory instability appears shrinks to the area above the dashed line. As the distribution of synaptic times widens, the stationary state becomes more stable. The introduction of random synaptic times also slightly reduces the frequency of the oscillation.

The critical line is thus quite sensitive to the distribution of synaptic times. In fact, distributions of synaptic times can be found such that the stationary state is always stable (e.g., for an exponential distribution $\Pr(\delta) = \exp(-\delta/\delta_0)/\delta$).

4.2 Effect of Inhomogeneous Connectivity. The analysis can also be extended to the case when the number of connections impinging on a neuron is no longer fixed at C, but rather connections are drawn at random independently at each site. In that case, the number of connections received by a neuron is a random variable with mean C and standard deviation $\sim \sqrt{C}$. This inhomogeneity in the connectivity provokes a significant inhomogeneity in the individual spike rates even for C large, because differences between the average input received by two neurons are of the same order as the SD of the synaptic input. The distribution of frequencies for an arbitrary network of excitatory and inhibitory neurons has been obtained in Amit and Brunel (1997b). The main steps leading to this distribution are described in Section A.5. Next we study how inhomogeneity affects the dynamical properties of the network. Figure 9 shows that the instability line is almost unaffected by the inhomogeneity. The frequency of the global oscillation is also very close to the one of the homogeneous case.
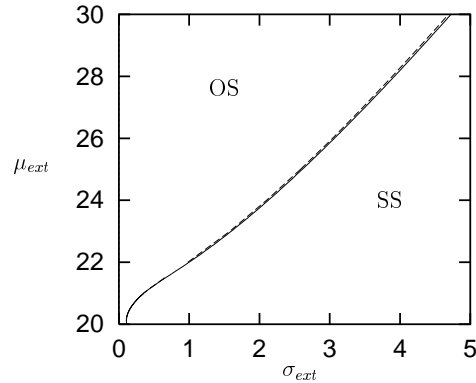
Figure 9: Effect of inhomogeneity in the connections on the instability line in the plane $(\mu_{ext}, \sigma_{ext})$ for $\tau = 20$ ms, $J = -0.1$ mV, $C = 1000$, $\theta = 20$ mV, $V_r = 10$ mV, $\delta = 2$ ms. Solid line: All neurons receive C connections. Dashed line: Connections are drawn randomly and independently at each synaptic site with probability C/N.

Amit and Brunel (1997b) showed by simulations that the degree of synchronization of a neuron with global activity is strongly affected by its spike rate: neurons with low firing frequencies tend to be more synchronized with the global activity than neurons with high frequencies. In Section A.5 we calculate analytically the degree of synchronization of individual neurons as a function of their frequency. The result is shown in Figure 10 in which the relative amplitude $C(\nu)$ of the cross-correlation between neurons firing at frequency ν and the global activity obtained analytically is compared with the result of simulations. It shows indeed that low-rate neurons are more synchronized with the global activity than high-rate neurons. The relative amplitude of the cross-correlation between two neurons of frequency ν_1 and ν_2 is given by the product of the two amplitudes, $C(\nu_1)C(\nu_2)$. Note that the heterogeneity in rates and cross-correlations is not very pronounced here, because near the critical line, the fluctuations in the external input dominate the local fluctuations, which tends to suppress this heterogeneity. In a network with both excitatory and inhibitory neurons with an external excitatory input of the same order as the internal excitatory contribution, this heterogeneity is much more pronounced (Amit & Brunel, 1997b).

4.3 Effect of More Realistic Synaptic Responses. Our analysis has been carried out for synaptic currents described by a delta pulse. One may wonder how the analysis generalizes for more realistic postsynaptic currents. We consider a function $f(t)$ describing the shape of the postsynaptic current when a spike is emitted at time $t = 0$ (see, e.g., Gerstner, 1995, for a review
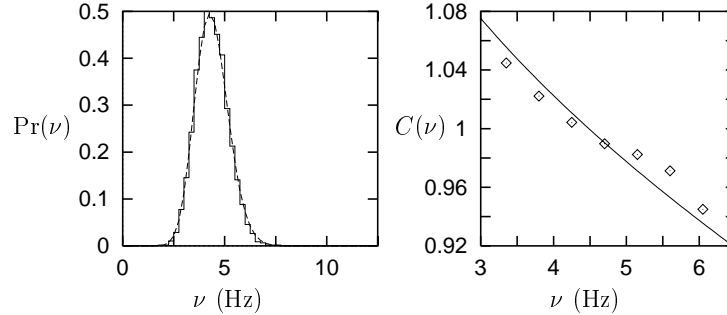
Figure 10: (Left) Distribution of spike rates (histogram: simulation; dashed line: theory). The distribution is similar to a gaussian, unlike the distributions observed in Amit & Brunel (1997b), which are much wider due to the balance between excitation and inhibition. (Right) Relative amplitude of CC between individual neurons and the global activity versus neuronal firing rate (diamonds: simulation; solid line: theory). $\tau = 20$ ms, $J = -0.1$ mV, $C = 1000$, $\theta = 20$ mV, $V_r = 10$ mV, $\delta = 2$ ms, $\mu_{ext} = 25$ mV, $\sigma_{ext} = 2.58$ mV.

of different types of synaptic responses). $f(t)$ is chosen such as

$$\int dt\, f(t) = 1.$$

An example often used in modeling studies and shown in Figure 2 is the α-function with a latency τ_L and a characteristic synaptic time τ_S:

$$f(t) = \begin{cases} \frac{t-\tau_L}{\tau_S^2} \exp\left(-\frac{t-\tau_L}{\tau_S}\right) & \text{for } t > \tau_L \\ 0 & \text{otherwise.} \end{cases} \tag{4.1}$$

The total synaptic current arriving at neuron i is now

$$RI_i(t) = \tau \sum_j J_{ij} \sum_k f\left(t - t_j^k\right).$$

In the diffusion approximation the synaptic current becomes

$$RI_i(t) = \mu(t) + \Xi_i(t),$$

in which the average part is given as a function of the frequency ν and the synaptic response function f by

$$\mu(t) = \mu_{ext} - CJ \int dt'\, \nu(t') f(t - t')\tau.$$

On the other hand, the fluctuating part $\Xi_i(t)$ can no longer be approximated by a pure white noise and exhibits temporal correlations at the scale

of the width of the PSC function $f(t)$. These temporal correlations in the currents complicate the analysis significantly, since the evolution of the distribution of the membrane potentials is no longer given by a simple one-dimensional Fokker-Planck equation. For the case of the α-function, we would need to solve the problem described by a three-dimensional Fokker-Planck equation. Such an analysis is beyond the scope of this article. Here, we choose to ignore, as a first approximation, these temporal correlations. Thus we consider only the effect of the PSC function on the average synaptic currents. In this approximation, the effect of the PSC function becomes equivalent to that of a distribution of synaptic times in the delta pulse PSC case considered in section 4.1. For example, in the limit in which τ_S and τ_L are small compared to the integration time constant, the equations for the bifurcation point are

$$G = \sqrt{\omega}\left[2\frac{\tau_S}{\tau}\omega\cos\left(\omega\frac{\tau_L}{\tau_S}\right) + \left(1 - \frac{\tau_S^2}{\tau^2}\omega^2\right)\sin\left(\omega\frac{\tau_L}{\tau}\right)\right]$$

$$H = \left(1 - \frac{\tau_S^2}{\tau^2}\omega^2\right)\left[\cos\left(\omega\frac{\tau_L}{\tau}\right) + \sin\left(\omega\frac{\tau_L}{\tau}\right)\right]$$

$$+ 2\frac{\tau_S}{\tau}\omega\left[\cos\left(\omega\frac{\tau_L}{\tau}\right) - \sin\left(\omega\frac{\tau_L}{\tau}\right)\right]. \tag{4.2}$$

In the case $\tau_L = 0$ (zero latency) the equations simplify to

$$G = 2\sqrt{\omega}\frac{\tau_S}{\tau}\omega \tag{4.3}$$

$$H = 1 - \frac{\tau_S^2}{\tau^2}\omega^2 + 2\frac{\tau_S}{\tau}\omega. \tag{4.4}$$

In the case $H = 1$, the frequency of the oscillation near the bifurcation point is equal to $1/(\pi\tau_S)$. Note that the dependence of the frequency on τ_S in the α function PSC case is similar to the dependence on δ in the delta pulse PSC case, equation 3.19.

To check the validity of this approximation, we have performed numerical simulations with fixed latency $\tau_L = 2$ ms, varying the decay time constant of the inhibitory postsynaptic current τ_S. The results are shown in Figure 11. The approximate analysis predicts the frequency is in the region between the two full lines (corresponding to $H = 0$ and $H = 1$). Simulation results deviate from the approximate analysis at rather small values of τ_S because of the effect of temporal correlations in the synaptic currents, which have the same scale as the period of the oscillation. Nonetheless, the approximation gives a good qualitative picture of the dependence of the frequency on τ_S.

Note that the frequencies obtained in this way can be directly compared to the data of Whittington et al. (1995) and Traub et al. (1996) since the decay
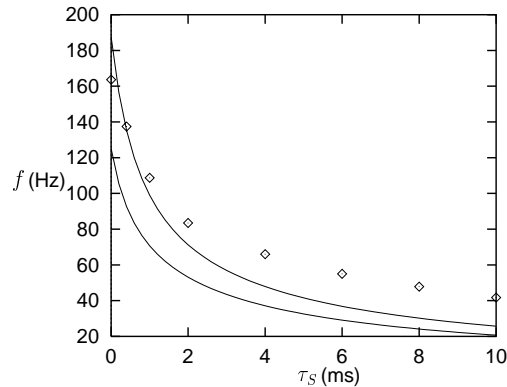
Figure 11: Dependence of the frequency of the oscillation near the bifurcation threshold on the synaptic decay time constant τ_S, for $\tau_L = 2$ ms. Network parameters as in Figure 3. External inputs have $\mu_{ext} = 25$ mV, $\sigma_{ext} = 2$ mV. This point is near the bifurcation line in the whole range of τ_S. $\diamond$: Simulations. Solid lines: Frequency given by the approximate analysis, equation 4.2, for $H = 1$ (lower curve), and $H = 0$ (upper curve).

time constant of the PSCs can be identified with their parameter τ_{GABA}. The frequencies obtained in the simulations are very close to the ones obtained in that study. For example, we obtain a frequency of about 40 Hz when $\tau_S = 10$ ms, in agreement with the in vitro recordings and the simulations of the more complex model of Whittington et al. (1995) and Traub et al. (1996). However, one has to be careful with such a comparison, since in that in vitro study, interneurons seem to fire at population frequency.

5 Conclusion

We have studied the existence of fast global oscillation in networks where individual neurons show irregular spiking at a low rate. We first showed that the phenomenon can be observed in a sparsely connected network composed of basic integrate-and-fire neurons. In this very simplified setting, the phenomenon has been precisely analyzed. At the simplest level, it differs from other modes of synchronization that lead to global oscillation in that recording at the individual neuron level shows a stochastic spike emission with nearly Poissonian interspike intervals and little indication of the collective behavior (see the ISI histograms in Figure 3). This oscillation regime has some similarity with that obtained in Wang et al. (1995), where a hyperpolarization-activated cation current seems to play the role of our random external inputs in generating intermittent activity in the network. This type of weak synchronization has sometimes been rationalized as coming

from filtering of external noise by recurrent inhibition (Traub et al., 1989). Our analysis leads to a somewhat different picture.

We have found that in the limit of an infinite network, the global oscillation is due to an oscillatory instability (a supercritical Hopf bifurcation) of the steady state. This instability occurs at a well-defined threshold and arises from the competition between the recurrent inhibition, which favors oscillations, and the intrinsic noise in the system, which tends to suppress it.

We found that the global oscillation period is controlled by the synaptic time. This appears to agree with previous experimental findings on slices of the rat hippocampus and with simulations results (Whittington et al., 1995; Traub et al., 1996), where it is, however, assumed that neurons fire at population frequency, unlike those of our model. A similar decrease in population frequency when the GABA characteristic time is varied is also observed in a recent in vitro experiment in which neurons fire sparsely (Fisahn et al., 1998). More work is necessary to clarify the relative roles of the different time constants (latency, IPSC rise time, IPSC decay time) that are commonly used to describe the synaptic response.

The oscillation period also depends on the characteristics of the external input, and particularly on the magnitude of the external noise, as shown by Figure 6. The initial rise in the frequency when one increases σ_{ext} followed by a saturation at sufficiently large σ_{ext} looks in fact similar to the dependence of the frequency on the amount of glutamate applied to hippocampal CA1 region in vitro (Traub et al., 1996). Our network is in a stationary state when external inputs are low and switches to an oscillatory regime when the magnitude of the external inputs is increased. This phenomenon resembles the induction of a gamma rhythm in the hippocampal slice mediated by carbachol (Fisahn et al., 1998), and the induction of faster 200 Hz rhythms, believed to be provoked by a massive excitation of CA1 cells through Schaeffer collaterals (see, e.g., Buzsáki et al., 1992). It is also interesting to note that a single network with fixed internal parameters is able to sustain collective oscillations in different frequency ranges when the characteristics of the external input are varied.

In a finite network, the sharp transition is smoothed, but the global oscillation has different characteristics above and below the critical threshold. Below threshold, its amplitude decreases as the network size is increased. Above threshold, an increase in the neuron number does not greatly modify the oscillation amplitude but increases its coherence time. It has been shown that the whole picture of a Hopf bifurcation with a well-defined threshold remains accurate when some of our simplifying assumptions are relaxed. It would be interesting to extend this finding to more realistic descriptions.

Our analysis also raises the important question of the synchronization mode used in real neural systems. Do neocortical or hippocampal neurons behave as oscillators with a frequency equal to the population frequency, or irregularly with firing rates lower than the population frequency? In hippocampus, pyramidal cells seem clearly to be in an irregular, low-rate

regime, during in vivo gamma (Bragin et al., 1995), in vivo 200 Hz (Buzsáki et al., 1992), and in vitro gamma oscillations (Fisahn et al., 1998). More recent experimental data indicate that interneurons also typically fire at a lower frequency than the population frequency during 200 Hz oscillations in CA1 (Csicsvari et al., 1998). Further experimental work is needed to clarify this important issue.

We have obtained a reduced description of the collective dynamics. The analysis can certainly be extended to more complicated networks, composed of neurons of different types or that are spatially extended. We hope that this reduced description will prove useful in clarifying the mechanisms of long-range synchrony and in studying propagation phenomena (Delaney et al., 1994; Prechtl, Cohen, Pesaran, Mitra, & Kleinfeld, 1997).

Finally, and most important, the exact roles of fast oscillations remain unclear. Are they useful for putting in resonance different neuronal populations, as it has been suggested? Can they serve to build a fast detector with slowly firing neurons? Are they used as a clock mechanism? Or do they reflect the usefulness of having a network where different neuronal populations fire in succession on a short timescale, to code spatial information in the temporal domain? Recent experiments (MacLeod & Laurent, 1996; Stopfer, Bhagavan, Smith, & Laurent, 1997) make us hope that elucidating the real meaning of these collective oscillations, at least in some neural systems, is an attainable goal. This is a question to which we hope to return in the future.

Appendix _____

The details of our computations are given in the following. We have found it convenient to use the rescaled variables,

$$P = \frac{2\tau v_0}{\sigma_0}Q, \;\; G = \frac{CJ\tau v_0}{\sigma_0} = \frac{\mu_{0,l}}{\sigma_0}, \;\; H = \frac{CJ^2\tau v_0}{\sigma_0^2} = \frac{\sigma_{0,l}^2}{\sigma_0^2}, \tag{A.1}$$

$$y = \frac{V - \mu_0}{\sigma_0}, \;\; y_\theta = \frac{\theta - \mu_0}{\sigma_0}, \;\; y_r = \frac{V_r - \mu_0}{\sigma_0}, \;\; v = v_0(1 + n(t)). \tag{A.2}$$

J and G are positive.

Using equations A.1 and A.2, the Fokker-Planck equation, 3.5, becomes

$$\tau \frac{\partial Q}{\partial t} = \mathcal{L}[Q] + v(t - \delta) \left(G \frac{\partial Q}{\partial y} + \frac{H}{2} \frac{\partial^2 Q}{\partial y^2} \right), \tag{A.3}$$

where the linear operator $\mathcal{L}$ is defined as

$$\mathcal{L}[Q] = \frac{1}{2} \frac{\partial^2 Q}{\partial y^2} + \frac{\partial}{\partial y}(yQ).$$

The equation is valid on the two intervals $-\infty < y < y_r$ and $y_r < y < y_\theta$. The boundary conditions at y_r and y_θ become: at y_θ,

$$Q(y_\theta, t) = 0, \quad \frac{\partial Q}{\partial y}(y_\theta, t) = -\frac{1 + n(t)}{1 + Hn(t - \delta)}; \tag{A.4}$$

at y_r,

$$[Q]_{y_r^-}^{y_r^+} = 0, \quad \left[\frac{\partial Q}{\partial y} \right]_{y_r^-}^{y_r^+} = -\frac{1 + n(t)}{1 + Hn(t - \delta)} \tag{A.5}$$

(the square bracket denotes the discontinuity of the function at y namely, $[f]_{y^-}^{y^+} \equiv \lim_{\epsilon \to 0}\{f(y + \epsilon) - f(y - \epsilon)\}$). Note that the terms on the r.h.s. of equations A.4 and A.5 are identical. Thus, when we study the Fokker-Planck equation at different orders, we will mention only the condition at y_θ. The condition at y_r can be obtained by replacing the value of the corresponding function at y_θ by the discontinuity of the function at y_r. Moreover $Q(y, t)$ should vanish sufficiently fast at $y = -\infty$ to be integrable.

The steady-state solution obeys

$$\mathcal{L}[Q_0] = 0 \tag{A.6}$$

and

$$\frac{\partial Q_0}{\partial y}(y_\theta) = -1, \quad \left[\frac{\partial Q_0}{\partial y} \right]_{y_r^-}^{y_r^+} = -1. \tag{A.7}$$

It is given by

$$Q_0(y) = \begin{cases} \exp(-y^2) \int_y^{y_\theta} du \, \exp(u^2) & y > y_r \\ \exp(-y^2) \int_{y_r}^{y_\theta} du \, \exp(u^2) & y < y_r. \end{cases} \tag{A.8}$$

From equations A.6 and A.7, one easily obtains the values of higher derivatives of Q_0 at $y = y_\theta$ and their discontinuities at $y = y_r$, which will be used in the following, using the recurrence relation

$$\frac{\partial^n Q_0}{\partial y^n}(y) = -2y \frac{\partial^{n-1} Q_0}{\partial y^{n-1}}(y) - 2(n - 1) \frac{\partial^{n-2} Q_0}{\partial y^{n-2}}(y). \tag{A.9}$$

A.1 Linear Stability. The function Q can be expanded around the steady-state solution $Q_0(y)$ as

$$Q(y) = Q_0(y) + Q_1(y, t) + Q_2(y, t) + \cdots$$

$$n(t) = n_1(t) + n_2(t) + \cdots \tag{A.10}$$

At first order, one obtains the linear equation

$$\tau \frac{\partial Q_1}{\partial t} = \mathcal{L}[Q_1] + n_1(t - \delta) \left(G \frac{dQ_0}{dy} + \frac{H}{2} \frac{d^2 Q_0}{dy^2} \right) \tag{A.11}$$

together with the boundary conditions

$$Q_1(y_\theta, t) = 0, \ \frac{\partial Q_1}{\partial y}(y_\theta) = -n_1(t) + Hn_1(t - \delta) \tag{A.12}$$

and

$$[Q_1]_{y_r^-}^{y_r^+} = 0, \ \left[\frac{\partial Q_1}{\partial y} \right]_{y_r^-}^{y_r^+} = -n_1(t) + Hn_1(t - \delta). \tag{A.13}$$

Eigenmodes of equation A.11 have a simple exponential behavior in time,

$$Q_1(y, t) = \exp(\lambda t/\tau) \, \hat{n}_1(\lambda) \hat{Q}_1(y, \lambda), \ n_1(t) = \exp(\lambda t/\tau) \, \hat{n}_1(\lambda),$$

and obey an ordinary differential equation in y,

$$\lambda \hat{Q}_1(y, \lambda) = \mathcal{L}[\hat{Q}_1](y, \lambda) + e^{-\lambda \delta/\tau} \left(G \frac{dQ_0}{dy} + \frac{H}{2} \frac{d^2 Q_0}{dy^2} \right), \tag{A.14}$$

together with the boundary conditions

$$\hat{Q}_1(y_\theta, t) = 0, \ \frac{\partial \hat{Q}_1}{\partial y}(y_\theta) = -1 + H \exp(-\lambda \delta/\tau),$$

and similar conditions at y_r.

The general solution of equation A.14 can be written as a linear superposition of two independent solutions $\phi_{1,2}$ of the homogeneous equation $1/2\phi'' + y\phi' + (1 - \lambda)\phi = 0$, plus a particular solution that can be obtained by differentiating equation A.6 with respect to y,

$$\hat{Q}_1(y, \lambda) = \begin{cases} \alpha_1^+(\lambda)\phi_1(y, \lambda) + \beta_1^+(\lambda)\phi_2(y, \lambda) + \hat{Q}_1^p(y, \lambda) & y > y_r \\ \alpha_1^-(\lambda)\phi_1(y, \lambda) + \beta_1^-(\lambda)\phi_2(y, \lambda) + \hat{Q}_1^p(y, \lambda) & y < y_r \end{cases} \tag{A.15}$$

with

$$\hat{Q}_1^p(y, \lambda) = e^{-\lambda\delta/\tau}\left(\frac{G}{1+\lambda}\frac{dQ_0(y)}{dy} + \frac{H}{2(2+\lambda)}\frac{d^2Q_0(y)}{dy^2}\right). \tag{A.16}$$

Solutions of the homogeneous equation $1/2\phi'' + y\phi' + (1-\lambda)\phi = 0$ can be obtained by their series expansion around $y = 0$. They are found to be a linear combination of two functions. The first one can be chosen as

$$\phi_1(y, \lambda) = 1 + \sum_{n=1}^{+\infty}(-1)^n\frac{(2y)^{2n}}{(2n)!}\prod_{k=0}^{n-1}\left(k + \frac{1-\lambda}{2}\right). \tag{A.17}$$

It coincides with the confluent hypergeometric function $M[(1-\lambda)/2, 1/2, -y^2]$ (see, e.g., Abramowitz & Stegun, 1970). A second independent solution can also be expressed in terms of the hypergeometric function M as

$$2yM\left(1 - \frac{\lambda}{2}, \frac{3}{2}, -y^2\right) = 2y + \sum_{n=1}^{+\infty}(-1)^n\frac{(2y)^{2n+1}}{(2n+1)!}\prod_{k=1}^{n}\left(k - \frac{\lambda}{2}\right). \tag{A.18}$$

The asymptotic behavior of both functions can conveniently be obtained from the following integral representations valid for $\mathrm{Re}(\lambda) < 1/2$,

$$\phi_1(y, \lambda) = \frac{1}{\Gamma(\frac{1-\lambda}{2})}\int_0^{+\infty}dt\,e^{-t}\cos(2y\sqrt{t})t^{-\frac{1+\lambda}{2}}$$

$$2yM\left(1 - \frac{\lambda}{2}, \frac{3}{2}, -y^2\right) = \frac{1}{\Gamma(1 - \frac{\lambda}{2})}\int_0^{+\infty}dt\,e^{-t}\sin(2y\sqrt{t})t^{-\frac{1+\lambda}{2}}. \tag{A.19}$$

(After replacing the cosine and sine in equation A.19 by their series expansions it is easily checked that the obtained series in powers of y^n coincide with equations A.17 and A.18.) The following asymptotic behaviors are found for $y \to -\infty$:

$$\phi_1(y, \lambda) \sim \frac{\sqrt{\pi}}{|y|^{1-\lambda}\Gamma(\lambda/2)} \tag{A.20}$$

$$2yM\left(1 - \frac{\lambda}{2}, \frac{3}{2}, -y^2\right) \sim -\frac{\sqrt{\pi}}{|y|^{1-\lambda}\Gamma[(1+\lambda)/2]}. \tag{A.21}$$

We find it convenient to choose $\phi_2(y, \omega)$ as the particular combination of these two functions that decays exponentially (i.e., like $|y|^{-\lambda}\exp(-y^2)$) at $y = -\infty$,

$$\phi_2(y, \omega) = \frac{\sqrt{\pi}}{\Gamma\left(\frac{1+\lambda}{2}\right)}M\left(\frac{1-\lambda}{2}, \frac{1}{2}, -y^2\right)$$

$$+ \frac{\sqrt{\pi}}{\Gamma\left(\frac{\lambda}{2}\right)}2yM\left(1 - \frac{\lambda}{2}, \frac{3}{2}, -y^2\right). \tag{A.22}$$

Thus for $\hat{Q}_1(y, t)$ to be integrable on $[-\infty, y_\theta]$ we need to require $\alpha_1^- = 0$ in equation A.15.

For further reference, we give the asymptotic behavior for $\lambda_2 = \text{Im}(\lambda) \to +\infty$,

$$\phi_1(y, \lambda_1 + i\lambda_2) \sim \cosh\left[y\sqrt{\lambda_2 - i\lambda_1}(1 + i)\right] \exp(-y^2/2) \qquad (\text{A.23})$$

$$\phi_2(y, \lambda_1 + i\lambda_2) \sim \frac{\sqrt{\pi}}{\Gamma\left(\frac{1+\lambda}{2}\right)} \exp\left[y\sqrt{\lambda_2 - i\lambda_1}(1 + i) - y^2/2\right], \qquad (\text{A.24})$$

where the determination of the square root is fixed by requiring it to be positive for $\lambda_1 = 0$.

Finally, we note that the Wronskian Wr of ϕ_1 and ϕ_2 obeys the first-order equation $\text{Wr}' = -2y\text{Wr}$ and therefore has the simple expression

$$\text{Wr}(\phi_1, \phi_2) \equiv \phi_1 \phi_2' - \phi_1' \phi_2 = \frac{2\sqrt{\pi}}{\Gamma(\lambda/2)} \exp(-y^2) \qquad (\text{A.25})$$

(the prefactor being fixed by equations A.23 and A.24).

The four boundary conditions, equations A.12 and A.13, give a linear system of four equations for the four remaining unknowns $\alpha_1^+, \alpha_1^-, \beta_1^+$, and β_1^-. The condition $\alpha_1^- = 0$ needed to obtain an integrable $\hat{Q}_1(y, t)$ gives the eigenfrequencies of the linear equation, A.11. To obtain the required solvability condition and the allied solutions, we find it convenient to use first the two boundary conditions (see equation A.12) to obtain α_1^+ and β_1^+. This gives

$$\alpha_1^+ = \frac{1}{\text{Wr}(y_\theta)} \left\{ \phi_2(y_\theta)(1 - He^{-\lambda\delta/\tau}) - W_2\left[\hat{Q}_1^p\right](y_\theta) \right\} \qquad (\text{A.26})$$

$$\beta_1^+ = -\frac{1}{\text{Wr}(y_\theta)} \left\{ \phi_1(y_\theta)(1 - He^{-\lambda\delta/\tau}) - W_1\left[\hat{Q}_1^p\right](y_\theta) \right\}, \qquad (\text{A.27})$$

where Wr denotes the Wronskian of ϕ_1 and ϕ_2, equation A.25, and $W_j(j = 1, 2)$ the Wronskian of the function in its argument and $\phi_{1,2}$

$$W_j\left[\hat{Q}\right] \equiv \hat{Q}\phi_j' - \hat{Q}'\phi_j \text{ for } j = 1, 2.$$

For matters of convenience we define $\tilde{\phi}_{1,2}$ and $\tilde{W}_{1,2}$ by

$$\tilde{\phi}_{1,2} = \frac{\phi_{1,2}}{\text{Wr}}, \quad \tilde{W}_{1,2}\left[\hat{Q}_1^p\right] = \frac{W_{1,2}\left[\hat{Q}_1^p\right]}{\text{Wr}}.$$

The two boundary conditions at $y = y_r$ (see equation A.13) give similar equations for $\alpha_1^+ - \alpha_1^-$ and $\beta_1^+ - \beta_1^-$ with y_θ replaced by y_r

$$\alpha_1^- = \alpha_1^+ - \tilde{\phi}_2(y_r)(1 - He^{-\lambda\delta/\tau}) - \left[\tilde{W}_2\left[\hat{Q}_1^p\right](y)\right]_{y_r^-}^{y_r^+} \tag{A.28}$$

$$\beta_1^- = \beta_1^+ + \tilde{\phi}_1(y_r)(1 - He^{-\lambda\delta/\tau}) - \left[\tilde{W}_1\left[\hat{Q}_1^p\right](y)\right]_{y_r^-}^{y_r^+}.$$

Equations A.26 and A.28 together with $\alpha_1^- = 0$ give the solvability condition and the equation for the eigenfrequencies of equation A.11:

$$\left(\tilde{\phi}_2(y_\theta) - \tilde{\phi}_2(y_r)\right)(1 - He^{-\lambda\delta/\tau}) = \tilde{W}_2\left[\hat{Q}_1^p\right](y_\theta)$$

$$- \left[\tilde{W}_2\left[\hat{Q}_1^p\right](y)\right]_{y_r^-}^{y_r^+}. \tag{A.29}$$

When the synaptic time δ becomes much smaller than τ, the roots λ of this equation become large. Considering for definiteness roots $\lambda = \lambda_1 + i\lambda_2$ with $\lambda_2 > 0$, in the limit $|\lambda| \to +\infty$, $\lambda_2 \to +\infty$, one obtains from equation A.24 that $\partial_y\phi_2(y_\theta) \gg \partial_y\phi_2(y_r)$ and $\partial_y\phi_2(y_\theta) \sim \sqrt{\lambda_2 - i\lambda_1}(1 + i)\phi_2$. We then note that for equation A.29 to have such a root, we need $G \sim \sqrt{|\lambda|}$. Since $H < 1$ by definition, we can neglect the terms proportional to H in $\hat{Q}_1^p$ and finally obtain

$$G\frac{e^{-\lambda\delta/\tau}}{\lambda}\sqrt{\lambda_2 - i\lambda_1}(1 + i) = -1 + He^{-\lambda\delta/\tau}. \tag{A.30}$$

We focus on the root with the largest real part (together with its complex conjugate). Its real part becomes positive, $\lambda = i\lambda_2 = i\omega_c$, when

$$1 - He^{-i\omega_c\delta/\tau} + \frac{(1 - i)Ge^{-i\omega_c\delta/\tau}}{\sqrt{\omega_c}} = 0,$$

that is,

$$G = \sqrt{\omega_c}\sin\left(\omega_c\delta/\tau\right)$$

$$H = \sin\left(\omega_c\delta/\tau\right) + \cos\left(\omega_c\delta/\tau\right).$$

A.2 Weakly Nonlinear Analysis. Our aim is to determine the lowest nonlinear terms that saturate the instability that appears when one crosses the critical line in the plane μ_{ext}, σ_{ext}. This determines the amplitude of the collective oscillation as well as the nonlinear contribution to its frequency in the vicinity of (G_c, H_c). We follow the usual strategy of pushing the development (see equation A.10) to higher order. One finds that the nth-order

term obeys inhomogeneous linear equations with forcing terms formed by quadratic combinations of lowest-order terms. We first determine the second-order terms that are forced by quadratic combination of first-order terms and therefore oscillate at 0 and $2\omega_c$. At third order, the coupling between first- and second-order terms generates forcing terms at ω_c and $3\omega_c$. While there is no problem determining the $3\omega_c$ contribution, the ω_c forcing is resonant and generates secular terms. The dynamics of the first-order terms amplitude is determined by the requirement that it cancel the unwanted secular contribution. The computation is not especially difficult, but it is rather long.

We substitute the developments (see equation A.10) of $Q(y, t)$ and $n(t)$ in equation 3.15, anticipating that the development parameter is of order of the square root of the differences $G - G_c$, $H - H_c$. Departure of G from G_c and of H from H_c will therefore affect only the third-order terms.

The first-order terms have already been obtained,

$$Q_1(y, t) = e^{i\omega_c t/\tau} \hat{n}_1 \hat{Q}_1(y, i\omega_c) + \text{c.c.}$$

$$n_1(t) = e^{i\omega_c t/\tau} \hat{n}_1(i\omega_c) + \text{c.c.}, \tag{A.31}$$

where $\hat{Q}_1$ is given by equations A.15, A.16, A.26, and A.27. In equation A.31, we recall that c.c. means that complex conjugate terms to those explicitly written have to be added. In the following, we omit the explicit mention of the variable λ to lighten the notation since functions of λ will all be evaluated at $i\omega_c$ (except when explicitly specified otherwise).

By differentiation of equation A.11 one can easily obtain recursively the values of higher derivatives of $\hat{Q}_1$ at $y = y_\theta$ and their discontinuities at $y = y_r$, which will be used in the following.

A.2.1 Second Order. We first determine the second-order terms. They obey the equation

$$\tau \frac{\partial Q_2}{\partial t} = \mathcal{L}[Q_2] + n_2(t - \delta) \left(G_c \frac{dQ_0}{dy} + \frac{H_c}{2} \frac{d^2 Q_0}{dy^2} \right)$$

$$+ n_1(t - \delta) \left(G_c \frac{\partial Q_1}{\partial y} + \frac{H_c}{2} \frac{\partial^2 Q_1}{\partial y^2} \right) \tag{A.32}$$

together with the boundary conditions

$$Q_2(y_\theta, t) = 0, \frac{\partial Q_2}{\partial y}(y_\theta) = -n_2(t) + Hn_2(t - \delta) - H^2 n_1^2(t - \delta)$$

$$+ Hn_1(t)n_1(t - \delta) \tag{A.33}$$

and a similar condition in y_r.

From equation A.31, the forcing term on the r.h.s of equation A.32 contains terms at frequencies $2\omega_c$ and 0. Therefore, we search $Q_2(y, t)$ and $n_2(t)$ under the form

$$Q_2(y, t) = e^{2i\omega_c t/\tau} \hat{n}_1^2 \hat{Q}_{2,2}(y) + e^{-2i\omega_c t/\tau} (\hat{n}_1^*)^2 \hat{Q}_{2,2}^*(y) + \hat{Q}_{2,0}|\hat{n}_1|^2 \quad \text{(A.34)}$$

$$n_2(t) = e^{2i\omega_c t/\tau} \hat{n}_1^2 \rho_{2,2} + e^{-2i\omega_c t/\tau} (\hat{n}_1^*)^2 \rho_{2,2}^{\star} + |\hat{n}_1|^2 \rho_{2,0}. \quad \text{(A.35)}$$

Substitution of equation A.35 into A.32 shows that $\hat{Q}_{2,2}$ obeys the ordinary differential equation,

$$(2i\omega_c - L)\hat{Q}_{2,2}(y) = \rho_{2,2} e^{-2i\omega_c \delta/\tau} \left(G_c \frac{dQ_0}{dy} + \frac{H_c}{2} \frac{d^2 Q_0}{dy^2} \right)$$

$$+ e^{-i\omega_c \delta/\tau} \left(G_c \frac{\partial \hat{Q}_1}{\partial y} + \frac{H_c}{2} \frac{\partial^2 \hat{Q}_1}{\partial y^2} \right), \quad \text{(A.36)}$$

together with the boundary conditions

$$\hat{Q}_{2,2}(y_\theta, t) = 0, \frac{\partial \hat{Q}_{2,2}}{\partial y}(y_\theta) = -\rho_{2,2} + He^{-2i\omega_c \delta/\tau} \rho_{2,2}$$

$$- H^2 e^{-2i\omega_c \delta/\tau} + He^{-i\omega_c \delta/\tau}$$

and a similar condition in y_r.

As above, the general solution of equation A.36 is written as a superposition of solution of the homogeneous equation and a particular solution

$$\hat{Q}_{2,2}(y) = \begin{cases} \alpha_2^+ \phi_1(y, 2i\omega_c) + \beta_2^+ \phi_2(y, 2i\omega_c) \\ \quad + \rho_{2,2}\hat{Q}_{2,2}^{so} + \hat{Q}_{2,2}^{lo} & y > y_r \\ \alpha_2^- \phi_1(y, 2i\omega_c) + \beta_2^- \phi_2(y, 2i\omega_c) \\ \quad + \rho_{2,2}\hat{Q}_{2,2}^{so} + \hat{Q}_{2,2}^{lo} & y < y_r \end{cases} \quad \text{(A.37)}$$

where

$$\hat{Q}_{2,2}^{so} = e^{-2i\omega_c \delta/\tau} \left(\frac{G_c}{1 + 2i\omega_c} \frac{dQ_0}{dy} + \frac{H_c}{4(1 + i\omega_c)} \frac{d^2 Q_0}{dy^2} \right).$$

$\hat{Q}_{2,2}^{lo}$ can be obtained by differentiation of Q_0 and $\hat{Q}_1$ using equations A.6 and A.14 and involves only terms of lower order that have already

been determined,

$$\hat{Q}_{2,2}^{lo}(y) = e^{-i\omega_c\delta/\tau}\left(\frac{G_c}{1+i\omega_c}\frac{\partial\hat{Q}_1}{\partial y} + \frac{H_c}{2(2+i\omega_c)}\frac{\partial^2\hat{Q}_1}{\partial y^2}\right)$$

$$- e^{-2i\omega_c\delta/\tau}\left(\frac{G_c^2}{2(1+i\omega_c)^2}\frac{d^2Q_0}{dy^2} + \frac{H_cG_c}{2(1+i\omega_c)(2+i\omega_c)}\frac{d^3Q_0}{dy^3}\right.$$

$$\left. + \frac{H_c^2}{8(2+i\omega_c)^2}\frac{d^4Q_0}{dy^4}\right).$$

The four boundary conditions for $\hat{Q}_2$ determine the four unknowns $\alpha_2^+, \beta_2^+, \beta_2^-, \alpha_2^-$ in terms of $\rho_{2,2}$ and the previously determined functions. With the integrability condition $\alpha_2^- = 0$, we obtain that $\rho_{2,2}$ is equal to

$$\frac{\begin{array}{c}(\tilde{\phi}_2(y_\theta) - \tilde{\phi}_2(y_r))H_ce^{-i\omega_c\delta/\tau}(1 - H_ce^{-i\omega_c\delta/\tau}) \\ + \tilde{W}_2[\hat{Q}_{2,2}^{lo}](y_\theta) - [\tilde{W}_2[\hat{Q}_{2,2}^{lo}](y)]_{y_r^-}^{y_r^+}\end{array}}{\begin{array}{c}(\tilde{\phi}_2(y_\theta) - \tilde{\phi}_2(y_r))(1 - H_ce^{-2i\omega_c\delta/\tau}) \\ - \tilde{W}_2[\hat{Q}_{2,2}^{so}](y_\theta) + [\tilde{W}_2[\hat{Q}_{2,2}^{so}](y)x]_{y_r^-}^{y_r^+}\end{array}},$$

in which all functions are taken at argument $2i\omega_c$.

The component at frequency zero $\hat{Q}_{2,0}$ obeys

$$0 = \mathcal{L}[\hat{Q}_{2,0}] + \rho_{2,0}\left(G_c\frac{dQ_0}{dy} + \frac{H_c}{2}\frac{d^2Q_0}{dy^2}\right)$$

$$+ \left[e^{-i\omega_c\delta/\tau}\left(G_c\frac{\partial\hat{Q}_1^\star}{\partial y} + \frac{H_c}{2}\frac{\partial^2\hat{Q}_1^\star}{\partial y^2}\right) + \text{c.c.}\right], \qquad (A.38)$$

together with the boundary conditions

$$\hat{Q}_{2,0}(y_\theta, t) = 0, \frac{\partial\hat{Q}_{2,0}}{\partial y}(y_\theta) = -\rho_{2,0}(1 - H) - 2H^2\cos(\omega_c\delta/\tau)$$

and a similar condition in y_r.

Its general solution can be written

$$\hat{Q}_{2,0}(y) = \begin{cases} \alpha_{2,0}^+ Q_0 + \beta_{2,0}^+\exp(-y^2) + \rho_{2,0}\hat{Q}_{2,0}^{so}(y) \\ \quad + \hat{Q}_{2,0}^{lo}(y) & y > y_r \\ \alpha_{2,0}^- Q_0 + \beta_{2,0}^-\exp(-y^2) + \rho_{2,0}\hat{Q}_{2,0}^{so}(y) \\ \quad + \hat{Q}_{2,0}^{lo}(y) & y < y_r, \end{cases} \qquad (A.39)$$

where

$$\hat{Q}_{2,0}^{so}(y) = \left(G_c \frac{dQ_0}{dy} + \frac{H_c}{4} \frac{d^2Q_0}{dy^2} \right),$$

and it is again convenient to construct the particular solution $Q_{2,0}^{lo}$ by differentiation

$$\hat{Q}_{2,0}^{lo}(y) = \left[e^{+i\omega_c\delta/\tau} \left(\frac{G_c}{1 - i\omega_c} \frac{\partial\hat{Q}_1}{\partial y} + \frac{H_c}{2(2 - i\omega_c)} \frac{\partial^2\hat{Q}_1}{\partial y^2} \right) + \text{c.c.} \right]$$
$$- \left(\frac{G_c^2}{1 + \omega_c^2} \frac{d^2Q_0}{dy^2} + \frac{H_c G_c(2 + \omega_c^2)}{(1 + \omega_c^2)(4 + \omega_c^2)} \frac{d^3Q_0}{dy^3} \right.$$
$$\left. + \frac{H_c^2}{4(4 + \omega_c^2)} \frac{d^4Q_0}{dy^4} \right). \tag{A.40}$$

In this case, the four boundary conditions for $\hat{Q}_{2,0}$ are not independent and are not sufficient to determine the four unknowns $\alpha_{2,0}^+, \alpha_{2,0}^-, \beta_{2,0}^+, \beta_{2,0}^-$ in functions of lower-order terms. This comes about because some choices of $Q_{2,0}$ are equivalent to changing the normalization of Q_0. One should therefore eliminate them by imposing the condition $\int_{-\infty}^{y_\theta} dy\hat{Q}_{2,0} = 0$. In this way, one obtains,

$$\rho_{2,0} = \frac{\left[\left(-2\frac{G_c}{1+\omega_c^2}\gamma_G + \frac{H_c}{4+\omega_c^2}\gamma_H \right) e^{y^2} \int_{-\infty}^y du e^{-u^2} \right]_{y_r}^{y_\theta} + \gamma_I}{\frac{1}{2v_0} + \left[\left(G_c - \frac{H_c y}{2} \right) e^{y^2} \int_{-\infty}^y du e^{-u^2} \right]_{y_r}^{y_\theta}}, \tag{A.41}$$

where

$$\gamma_G(y) = G_c y + \cos(\omega_c\delta/\tau) - \omega_c \sin(\omega_c\delta/\tau) - \frac{H_c(2y^2 + 1)}{3}$$

$$\gamma_H(y) = 4y\cos(\omega_c\delta/\tau) - 2y\omega_c \sin(\omega_c\delta/\tau) + \frac{4G_c(2y^2 + 1)}{3}$$
$$- H_c(2y^3 + 3y)$$

$$\gamma_I = -2(y_\theta - y_r)G_c H_c \frac{2 + \omega_c^2}{(1 + \omega_c^2)(4 + \omega_c^2)} + \frac{H_c^2(y_\theta^2 - y_r^2)}{4 + \omega_c^2}$$

(the notation $[f]_{y_r}^{y_\theta} \equiv f(y_\theta) - f(y_r)$ is used). The derivatives of higher order of $\hat{Q}_{2,2}$ and $\hat{Q}_{2,0}$, which are used in the following, can be obtained recursively by differentiation of equations A.36 and A.38.

A.2.2 Third Order.   We can now proceed and study the third-order terms.
They obey the equation

$$\tau \frac{\partial Q_3}{\partial t} = \mathcal{L}[Q_3] + n_3(t - \delta) \left(G_c \frac{dQ_0}{dy} + \frac{H_c}{2} \frac{d^2Q_0}{dy^2} \right)$$

$$+ n_2(t - \delta) \left(G_c \frac{\partial Q_1}{\partial y} + \frac{H_c}{2} \frac{\partial^2 Q_1}{\partial y^2} \right)$$

$$+ n_1(t - \delta) \left(G_c \frac{\partial Q_2}{\partial y} + \frac{H_c}{2} \frac{\partial^2 Q_2}{\partial y^2} \right)$$

$$+ n_1(t - \delta) \left((G - G_c) \frac{dQ_0}{dy} + \frac{(H - H_c)}{2} \frac{d^2Q_0}{dy^2} \right)$$

$$- \left\{ \tau \frac{d\hat{n}_1}{dt} \hat{Q}_1 e^{i\omega_c t/\tau} \right.$$

$$\left. + \delta \frac{d\hat{n}_1}{dt} e^{i\omega_c(t - \delta)/\tau} \left(G_c \frac{dQ_0}{dy} + \frac{H_c}{2} \frac{d^2Q_0}{dy^2} \right) + \text{c.c.} \right\}, \quad \text{(A.42)}$$

together with boundary conditions

$$\hat{Q}_3(y_\theta) = 0$$

$$\frac{\partial \hat{Q}_3}{\partial y}(y_\theta) = -n_3(t) + H n_3(t - \delta) - 2H^2 n_1(t - \delta) n_2(t - \delta)$$

$$+ H \left(n_1(t) n_2(t - \delta) + n_1(t - \delta) n_2(t) \right) + H^3 n_1^3(t - \delta)$$

$$- H^2 n_1(t) n_1^2(t - \delta) + (H - H_c) n_1(t - \delta)$$

$$- H \delta \frac{d\hat{n}_1}{dt} e^{i\omega_c(t - \delta)/\tau}, \quad \text{(A.43)}$$

and a similar condition holds at y_r.

The last two terms between brackets on the r.h.s. of equation A.42 come
from the anticipation that it will be needed to have $\hat{n}_1$ change on a slow
timescale to cancel secular terms. The first term arises from the explicit
time differentiation in equation A.3 and does not need special explanation.
The second is less usual and comes from the delayed forcing $v(t - \delta)$ in
equation A.3. Formally introducing a slow timescale $T = \epsilon t$, the delayed
forcing is written $v(t - \delta, T - \epsilon \delta)$. The second term between brackets in
equation A.42 is produced by the expansion to first order in ϵ $v(t - \delta, T - \epsilon \delta) = v(t - \delta) - \epsilon \delta \, \partial_T v(t - \delta) + \cdots$ The last term in the boundary condition,
equation A.43, appears in the same way.

The forcing terms on the r.h.s. of equation A.42, oscillate at frequencies $3\omega_c$ and ω_c. Therefore, we search $Q_3(y,t)$ and $n_3(t)$ under the form

$$Q_3(y,t) = e^{3i\omega_c t/\tau}\hat{Q}_{3,3}(y) + e^{i\omega_c t/\tau}\hat{Q}_{3,1}(y) + \text{c.c.}$$
$$n_3(t) = e^{3i\omega_c t/\tau}\hat{n}_{3,3} + e^{i\omega_c t/\tau}\hat{n}_{3,1} + \text{c.c.} \tag{A.44}$$

We focus on the terms at frequency ω_c, which are resonant with the first-order terms. They obey the equation

$$
(i\omega_c - L)\hat{Q}_{3,1}(y) = \hat{n}_{3,1}e^{-i\omega_c\delta/\tau}\left(G_c\frac{dQ_0}{dy} + \frac{H_c}{2}\frac{d^2Q_0}{dy^2}\right)
$$
$$
+ |\hat{n}_1|^2\hat{n}_1\left\{\rho_{22}e^{-2i\omega_c\delta/\tau}\left(G_c\frac{\partial\hat{Q}_1^\star}{\partial y} + \frac{H_c}{2}\frac{\partial^2\hat{Q}_1^\star}{\partial y^2}\right)\right.
$$
$$
+ \rho_{20}\left(G_c\frac{\partial\hat{Q}_1}{\partial y} + \frac{H_c}{2}\frac{\partial^2\hat{Q}_1}{\partial y^2}\right)
$$
$$
+ e^{-i\omega_c\delta/\tau}\left(G_c\frac{\partial\hat{Q}_{2,0}}{\partial y} + \frac{H_c}{2}\frac{\partial^2\hat{Q}_{2,0}}{\partial y^2}\right)
$$
$$
+ \left.e^{i\omega_c\delta/\tau}\left(G_c\frac{\partial\hat{Q}_{2,2}}{\partial y} + \frac{H_c}{2}\frac{\partial^2\hat{Q}_{2,2}}{\partial y^2}\right)\right\}
$$
$$
+ \hat{n}_1 e^{-i\omega_c\delta/\tau}\left((G-G_c)\frac{dQ_0}{dy} + \frac{(H-H_c)}{2}\frac{d^2Q_0}{dy^2}\right)
$$
$$
- \tau\frac{d\hat{n}_1}{dt}\hat{Q}_1
$$
$$
- e^{-i\omega_c\delta/\tau}\delta\frac{d\hat{n}_1}{dt}\left(G_c\frac{dQ_0}{dy} + \frac{H_c}{2}\frac{d^2Q_0}{dy^2}\right). \tag{A.45}
$$

The general solution of equation A.45 can be written

$$
\hat{Q}_3(y) = \begin{cases} \alpha_3^+\phi_1(y,i\omega_c) + \beta_3^+\phi_2(y,i\omega_c) + \hat{n}_{3,1}\hat{Q}_1^p + \hat{Q}_{3,1}^{lo} & y > y_r \\ \alpha_3^-\phi_1(y,i\omega_c) + \beta_3^-\phi_2(y,i\omega_c) + \hat{n}_{3,1}\hat{Q}_1^p + \hat{Q}_{3,1}^{lo} & y < y_r. \end{cases} \tag{A.46}
$$

In the particular solution, $\hat{Q}_1^p$ is the function that appears at first order, equation A.16, and as before, we can construct $\hat{Q}_{3,1}^{lo}$ by differentiation of lower-order terms:

$$
\hat{Q}_{3,1}^{lo} = \tau\frac{d\hat{n}_1}{dt}\hat{Q}_{3,1}^d + \hat{n}_1\hat{Q}_{3,1}^l + \hat{n}_1|\hat{n}_1|^2\hat{Q}_{3,1}^c, \tag{A.47}
$$

where $\hat{Q}_{3,1}^d$ is obtained from $\hat{Q}_1$ by differentiation of $\phi_{1,2}$ and $\hat{Q}_1^p$ with respect to λ:

$$\hat{Q}_{3,1}^d(y) = \begin{cases} \alpha_1^+ \partial_\lambda \phi_1(y, i\omega_c) + \beta_1^+ \partial_\lambda \phi_2(y, i\omega_c) \\ \quad + \partial_\lambda \hat{Q}_1^p(y, i\omega_c) & y > y_r \\ \beta_1^- \partial_\lambda \phi_2(y, i\omega_c) \\ \quad + \partial_\lambda \hat{Q}_1^p(y, i\omega_c) & y < y_r, \end{cases} \tag{A.48}$$

$$\hat{Q}_{3,1}^l = e^{-i\omega_c \delta/\tau} \left(\frac{(G - G_c)}{1 + i\omega_c} \frac{dQ_0}{dy} + \frac{(H - H_c)}{2(2 + i\omega_c)} \frac{d^2 Q_0}{dy^2} \right), \tag{A.49}$$

and

$$\hat{Q}_{3,1}^c = e^{i\omega_c \delta/\tau} \left(\frac{G_c}{1 - i\omega_c} \frac{\partial \hat{Q}_{2,2}}{\partial y} + \frac{H_c}{2(2 - i\omega_c)} \frac{\partial^2 \hat{Q}_{2,2}}{\partial y^2} \right)$$

$$+ e^{-i\omega_c \delta/\tau} \left(\frac{G_c}{1 + i\omega_c} \frac{\partial \hat{Q}_{2,0}}{\partial y} + \frac{H_c}{2(2 + i\omega_c)} \frac{\partial^2 \hat{Q}_{2,0}}{\partial y^2} \right)$$

$$+ \rho_{2,0} \left(G_c \frac{\partial \hat{Q}_1}{\partial y} + \frac{H_c}{4} \frac{\partial^2 \hat{Q}_1}{\partial y^2} \right)$$

$$+ \rho_{2,2} e^{-2i\omega_c \delta/\tau} \left(\frac{G_c}{1 + 2i\omega_c} \frac{\partial \hat{Q}_1^\star}{\partial y} + \frac{H_c}{4(1 + i\omega_c)} \frac{\partial^2 \hat{Q}_1^\star}{\partial y^2} \right)$$

$$- \frac{G_c}{1 + \omega_c^2} \left(G_c \frac{\partial^2 \hat{Q}_1}{\partial y^2} + \frac{H_c}{3} \frac{\partial^3 \hat{Q}_1}{\partial y^3} \right)$$

$$- 2 \frac{H_c}{4 + \omega_c^2} \left(\frac{G_c}{3} \frac{\partial^3 \hat{Q}_1}{\partial y^3} + \frac{H_c}{8} \frac{\partial^4 \hat{Q}_1}{\partial y^4} \right)$$

$$- e^{-2i\omega_c \delta/\tau} \frac{G_c}{1 + i\omega_c} \left(\frac{G_c}{2(1 + i\omega_c)} \frac{\partial^2 \hat{Q}_1^\star}{\partial y^2} + \frac{H_c}{2(3 + 2i\omega_c)} \frac{\partial^3 \hat{Q}_1^\star}{\partial y^3} \right)$$

$$- e^{-2i\omega_c \delta/\tau} \frac{H_c}{2(2 + i\omega_c)} \left(\frac{G_c}{3 + 2i\omega_c} \frac{\partial^3 \hat{Q}_1^\star}{\partial y^3} + \frac{H_c}{4(2 + i\omega_c)} \frac{\partial^4 \hat{Q}_1^\star}{\partial y^4} \right)$$

$$- \rho_{2,2} e^{-i\omega_c \delta/\tau} G_c \frac{2 + i\omega_c}{(1 - i\omega_c)(1 + 2i\omega_c)}$$

$$\left(\frac{G_c}{2 + i\omega_c} \frac{d^2 Q_0}{dy^2} + \frac{H_c}{2(3 + i\omega_c)} \frac{d^3 Q_0}{dy^3} \right)$$

$$- \rho_{2,0} e^{-i\omega_c \delta/\tau} G_c \frac{2 + i\omega_c}{1 + i\omega_c} \left(\frac{G_c}{2 + i\omega_c} \frac{d^2 Q_0}{dy^2} + \frac{H_c}{2(3 + i\omega_c)} \frac{d^3 Q_0}{dy^3} \right)$$

$$- \rho_{2,2} e^{-i\omega_c \delta/\tau} H_c \frac{4 + i\omega_c}{4(1 + i\omega_c)(2 - i\omega_c)}$$

$$\left(\frac{G_c}{3 + i\omega_c} \frac{dQ_0^3}{dy^3} + \frac{H_c}{2(4 + i\omega_c)} \frac{d^4 Q_0}{dy^4} \right)$$

$$- \rho_{2,0} e^{-i\omega_c \delta/\tau} H_c \frac{4 + i\omega_c}{4(2 + i\omega_c)} \left(\frac{G_c}{3 + i\omega_c} \frac{d^3 Q_0}{dy^3} + \frac{H_c}{2(4 + i\omega_c)} \frac{d^4 Q_0}{dy^4} \right)$$

$$+ e^{-i\omega_c \delta/\tau} G_c^2 \frac{3 + i\omega_c}{2(1 - i\omega_c)(1 + i\omega_c)^2}$$

$$\left(\frac{G_c}{3 + i\omega_c} \frac{d^3 Q_0}{dy^3} + \frac{H_c}{2(4 + i\omega_c)} \frac{d^4 Q_0}{dy^4} \right)$$

$$+ e^{-i\omega_c \delta/\tau} \frac{G_c H_c}{6} \left(\frac{2}{1 + \omega_c^2} + \frac{4}{4 + \omega_c^2} + \frac{3}{(1 + i\omega_c)(2 + i\omega_c)} \right)$$

$$\left(\frac{G_c}{4 + i\omega_c} \frac{d^4 Q_0}{dy^4} + \frac{H_c}{2(5 + i\omega_c)} \frac{d^5 Q_0}{dy^5} \right)$$

$$+ e^{-i\omega_c \delta/\tau} H_c^2 \frac{6 + i\omega_c}{8(2 + i\omega_c)^2(2 - i\omega_c)}$$

$$\left(\frac{G_c}{5 + i\omega_c} \frac{d^5 Q_0}{dy^5} + \frac{H_c}{2(6 + i\omega_c)} \frac{d^6 Q_0}{dy^6} \right). \tag{A.50}$$

Now, upon replacing $\alpha_3^- = 0$ one can try to determine $\alpha_3^+, \beta_3^+, \beta_3^-, \hat{n}_3$ from the four boundary conditions on $\hat{Q}_{3,1}(y)$. This provides a linear inhomogeneous system for the four unknowns. The inhomogeneous terms are made from $\hat{Q}_{3,1}^{lo}(y)$ and its derivatives evaluated at y_θ and y_r. But there is a difficulty: since we are considering the resonant part of the third-order terms, the linear operator coincides with the 4×4 matrix obtained at first order, which has been required to have a zero determinant. So the equations for $\alpha_3^+, \beta_3^+, \beta_3^-, \hat{n}_3$ are solvable only if the inhomogeneous terms obey a solvability condition. In order to obtain it, we find it convenient to proceed as we did at linear order (see equations A.26 and A.28). We obtain α_3^+ and β_3^+ in terms of $\hat{n}_{3,1}$ and $\hat{Q}_3^{lo}$ from the 2×2 system given by the two boundary conditions at y_θ. We then obtain similar expressions for α_3^+ and $\beta_3^+ - \beta_3^-$. Comparing the two obtained expressions for α_3^+ and requiring them to be identical provides the solvability condition,

$$\left(\tilde{\phi}_2(y_\theta) - \tilde{\phi}_2(y_r) \right) \Omega = \tilde{W}_2 \left[\hat{Q}_{3,1}^{lo} \right] (y_\theta) - \left[\tilde{W}_2 \left[\hat{Q}_{3,1}^{lo} \right] (y) \right]_{y_r^-}^{y_r^+}, \tag{A.51}$$

where

$$\Omega = -\frac{\delta}{\tau}He^{-i\omega_c\delta/\tau}\frac{d\hat{n}_1}{dt} - \hat{n}_1\Omega_1 - \hat{n}_1|\hat{n}_1|^2\Omega_3$$

$$\Omega_1 = (H - H_c)e^{-i\omega_c\delta/\tau}$$

$$\Omega_3 = -2H_c^2 e^{-i\omega_c\delta/\tau}(\rho_{22} + \rho_{20}) + 3H_c^3 e^{-i\omega_c\delta/\tau}$$
$$+ H_c\left[\rho_{22}(e^{-2i\omega_c\delta/\tau} + e^{i\omega_c\delta/\tau}) + \rho_{20}(1 + e^{-i\omega_c\delta/\tau})\right]$$
$$- H_c^2(2 + e^{-2i\omega_c\delta/\tau}). \tag{A.52}$$

With the help of equations A.47–A.50, this gives the searched-for equation of motion for $\hat{n}_1$

$$\tau\frac{d\hat{n}_1}{dT} = A\hat{v}_1 - B|\hat{v}_1|^2\hat{v}_1, \tag{A.53}$$

in which

$$A = \frac{-\tilde{W}_2[\hat{Q}_{3,1}^l](y_\theta) + [\tilde{W}_2[\hat{Q}_{3,l}^l](y)]_{y_r^-}^{y_r^+} - (\tilde{\phi}_2(y_\theta) - \tilde{\phi}_2(y_r))\Omega_1}{\tilde{W}_2[\hat{Q}_{3,1}^d](y_\theta) - [\tilde{W}_2[\hat{Q}_{3,1}^d](y)]_{y_r^-}^{y_r^+} + (\tilde{\phi}_2(y_\theta) - \tilde{\phi}_2(y_r))\frac{\delta}{\tau}He^{-i\omega_c\delta/\tau}} \tag{A.54}$$

$$B = \frac{\tilde{W}_2[\hat{Q}_{3,1}^c](y_\theta) - [\tilde{W}_2[\hat{Q}_{3,1}^c](y)]_{y_r^-}^{y_r^+} + (\tilde{\phi}_2(y_\theta) - \tilde{\phi}_2(y_r))\Omega_3}{\tilde{W}_2[\hat{Q}_{3,1}^d](y_\theta) - [\tilde{W}_2[\hat{Q}_{3,1}^d](y)]_{y_r^-}^{y_r^+} + (\tilde{\phi}_2(y_\theta) - \tilde{\phi}_2(y_r))\frac{\delta}{\tau}He^{-i\omega_c\delta/\tau}}. \tag{A.55}$$

These expressions simplify in the limit $\delta/\tau \to 0$. In the particular case $H = 0$, one obtains equation 3.21.

A.3 Effect of Noise Due to Finite-Size Effects. Inserting the noise in equation A.42, we obtain

$$\tau\frac{d\hat{n}_1}{dt} = A\hat{n}_1 - B|\hat{n}_1|^2\hat{n}_1 + D\sqrt{\tau}\zeta(t), \tag{A.56}$$

in which A and B are given by equations A.54 and A.55, while D is

$$D = \eta\frac{-\tilde{W}_2\left[\hat{Q}_{noise}\right](y_\theta) + \left[\tilde{W}_2\left[\hat{Q}_{noise}\right](y)\right]_{y_r^-}^{y_r^+}}{\tilde{W}_2\left[\hat{Q}_{3,1}^d\right](y_\theta) - \left[\tilde{W}_2\left[\hat{Q}_{3,1}^d\right](y)\right]_{y_r^-}^{y_r^+}}, \tag{A.57}$$

where

$$\hat{Q}_{noise} = \frac{e^{-i\omega_c\delta/\tau}}{1 + i\omega_c}\frac{dQ_0}{dy}.$$

η is given by equation 3.25 and ζ is a complex white noise such that $\langle\zeta(t)\zeta^\star(t')\rangle = \delta(t - t')$.

The autocorrelation at zero time $C(0)$ is given by

$$C(0) = 1 + 2\langle|\hat{n}_1(t)|^2\rangle.$$

We deduce from equation A.56 the Fokker-Planck equation describing the evolution of the PDF of both real and imaginary parts of $\hat{n}_1$. This equation can be converted in an equation giving the stationary distribution $\Pr(\rho)$ of $\rho \equiv |\hat{n}_1|^2$. It satisfies

$$\frac{\partial}{\partial\rho}\left(|D|^2\rho\frac{\partial\Pr}{\partial\rho}\right) = \frac{\partial}{\partial\rho}\left(\left[2A_r\rho - 2B_r\rho^2\right]\Pr\right),$$

whose solution is

$$\Pr(\rho) = \frac{\exp\left(2\frac{A_r}{|D|^2}\rho - \frac{B_r}{|D|^2}\rho^2\right)}{\int_0^\infty \exp\left(2\frac{A_r}{|D|^2}R - \frac{B_r}{|D|^2}R^2\right)dR},$$

and the autocorrelation at zero lag is

$$C(0) = 1 + 2\frac{\int_0^\infty R\exp\left(2\frac{A_r}{|D|^2}R - \frac{B_r}{|D|^2}R^2\right)dR}{\int_0^\infty \exp\left(2\frac{A_r}{|D|^2}R - \frac{B_r}{|D|^2}R^2\right)dR}.$$

From this exact expression, it is not difficult to obtain expressions 3.27–3.29.

From equation A.56, one can compute the behavior of the autocorrelation function $C(s)$. Far below the critical line, $|\hat{n}_1|$ is small and, the nonlinear term can be neglected. It is then easy to obtain equation 3.30.

In the oscillatory regime far above the critical line, finite-size effects provoke fluctuations of activity around the oscillation described by equation 3.22. We consider a small perturbation, in both amplitude and phase, of the "pure" oscillation $\hat{n}_1 \to \hat{n}_1(1 + r)\exp(i\phi)$. r is the perturbation in amplitude, while ϕ is the perturbation in phase. To obtain the evolution equations for r and ϕ we apply standard stochastic calculus techniques (see, e.g., Gardiner, 1983, chap. 4), and obtain,

$$\tau\dot{r} = -A_r(2r + 3r^2 + r^3) + \epsilon\zeta_r + \epsilon^2\frac{1}{2(1 + r)}, \tag{A.58}$$

$$\tau\dot{\phi} = -\frac{B_iA_r}{B_r}(2r + r^2) + \epsilon\frac{\zeta_i}{1 + r} \tag{A.59}$$

in which $\epsilon = |D|/R$, and ζ_r, ζ_i are uncorrelated white noises. Note that the last term in the r.h.s. of equation A.58 appears (Gardiner, 1983, sec. 4.4.5) due to the fact that, upon discretizing equation A.56 with a small time step dt, $\phi(t+dt) - \phi(t)$ is of order $\sqrt{dt}$, not dt. The calculation of the autocorrelation in terms of r and ϕ gives, keeping only the dominant term,

$$C(s) = 1 + 2R^2 \langle \cos\left((\omega_c + \Delta\omega)s/\tau + \phi(t+s) - \phi(t)\right)\rangle.$$

In order to calculate the autocorrelation we need to calculate the distribution of $\Delta\phi(s) = \phi(t+s) - \phi(t)$. From equations A.58 and A.59, we find that, to leading order in ϵ, it has a gaussian distribution with mean 0 and variance

$$\gamma^2(s) = \frac{|D|^2}{2R^2}\left[\frac{s}{\tau} + \frac{B_i^2}{2B_r^2 A_r}\left\{\exp\left(-\frac{2A_r s}{\tau}\right) - 1 + \frac{2A_r s}{\tau}\right\}\right].$$

Averaging $\cos((\omega_c + \Delta\omega)s/\tau + \Delta\phi(s))$ with such a distribution yields

$$C(s) = 1 + 2R^2 \cos\left((\omega_c + \Delta\omega)s/\tau\right)\exp\left(-\gamma^2(s)/2\right).$$

We find a damped cosine function as below the critical lines, but now the damping factor is no longer a simple exponential. For small times $s \ll \tau/(B_r R^2)$, the damping is described by

$$\exp\left(-\frac{\gamma^2(s)}{2}\right) \sim \exp\left(-\frac{|D|^2}{4R^2}\frac{s}{\tau}\right),$$

while for long times $s \gg \tau/(B_r R^2)$

$$\exp\left(-\frac{\gamma^2(s)}{2}\right) \sim \exp\left(-\frac{|D|^2}{4R^2}\left(1 + \frac{B_i^2}{B_r^2}\right)\frac{s}{\tau}\right).$$

The damping time constant in both regimes is proportional to $1/|D|^2 \sim N/C$, that is, to the inverse of the connection probability. When N goes to infinity at C fixed, the coherence time of the oscillation increases linearly with N.

The next order in ϵ brings (after a rather tedious calculation) a small additional contribution to the variance, so that for long times

$$\exp\left(-\frac{\gamma^2(s)}{2}\right) = \exp\left(-\frac{|D|^2}{4R^2}\left(1 + \frac{B_i^2}{B_r^2}\right)\frac{s}{\tau}\left[1 + \frac{|D|^2}{2A_r} + O\left(|D|^4\right)\right]\right).$$

A.4 Randomly Distributed Synaptic Times. The calculations performed in the case in which all synaptic times have the same value can be repeated in the more general situation in which synaptic times are drawn randomly and independently at each site with distribution $\Pr(\delta)$. The difference is that in all equations where functions of δ appear, we need to integrate these functions with the PDF $\Pr(\delta)$. For example, we find that the critical line where

the instability appears is given by

$$(\tilde{\phi}_2(y_\theta) - \tilde{\phi}_2(y_r)) \left(1 - H \int \Pr(\delta) e^{-w\delta/\tau} d\delta\right) = \tilde{W}_2[\hat{Q}_1^p](y_\theta)$$
$$- [\tilde{W}_2[\hat{Q}_1^p](y)]_{y_r^-}^{y_r^+} , \quad \text{(A.60)}$$

in which

$$\hat{Q}_1^p(y, w) = \int \Pr(\delta) e^{-w\delta/\tau} d\delta$$
$$\times \left(\frac{G}{1+w} \frac{dQ_0(y)}{dy} + \frac{H}{2(2+w)} \frac{d^2 Q_0(y)}{dy^2}\right). \quad \text{(A.61)}$$

A.5 Inhomogeneous Networks

We now relax the constraint that the number of connections received by a neuron be precisely equal to C. The connections are randomly and independently drawn at each possible site. They are present with probability C/N. In this situation, the dynamics of different neurons will depend on this number of connections they receive: this number is now a random variable with mean C and variance $C(1 - \epsilon)$. For example, their frequency will be a decreasing function of the number of connections. The connectivity matrix is defined by $J_{ij} = Je_{ij}$ where for all $i, j\ e_{ij} = 1$ with probability ϵ. The distribution of frequencies in the stationary state in such a situation has been obtained, for the case of a network with both excitatory and inhibitory neurons, by Amit and Brunel (1997b). The distribution of stationary frequencies can be obtained as a special case of this analysis. We briefly recall here the main steps of this analysis before turning to the stability analysis.

Averaging the synaptic input only on the randomness of spike emission times of presynaptic neurons, we get that the mean and the variance of local inputs are given by

$$\mu_i = J\tau \sum_j e_{ij} v_j, \quad \sigma_i^2 = J^2 \tau \sum_j e_{ij} v_j.$$

Since the number of inputs to each neuron is very large, the spatial distribution of the variable $\sum_j e_{ij} v_j$, which completely determines the spatial distribution of μ and σ, will be close to a gaussian whose two first moments can be calculated as a function of the two first moments of the spatial

distribution of frequencies:

$$\left\langle \sum_j e_{ij} v_j \right\rangle = C\overline{v}$$

$$\left\langle \left(\sum_j e_{ij} v_j - C\overline{v} \right)^2 \right\rangle = C\left(\overline{v^2} - \epsilon \overline{v}^2 \right).$$

Thus the variable

$$z_i = \frac{\sum_j e_{ij} v_j - C\overline{v}}{\sqrt{C\left(\overline{v^2} - \epsilon \overline{v}^2 \right)}}$$

has a gaussian distribution, $\rho(z) = \exp(-z^2/2)/\sqrt{2\pi}$. Thus a neuron receives, with probability $\rho(z)$, a local input with moments

$$\mu(z) = -J\tau \left(C\overline{v} + z\sqrt{C\left(\overline{v^2} - \epsilon \overline{v}^2 \right)} \right) \tag{A.62}$$

and

$$\sigma^2(z) = J^2\tau \left(C\overline{v} + z\sqrt{C\left(\overline{v^2} - \epsilon \overline{v}^2 \right)} \right). \tag{A.63}$$

A.5.1 Distribution of Frequencies in Stationary State.   In the stationary state the frequency of a neuron with moments $\mu(z)$ and $\sigma(z)$ is given by

$$v_0(z) = \left(\tau\sqrt{\pi} \int_{\frac{V_r-\mu(z)}{\sigma(z)}}^{\frac{\theta-\mu(z)}{\sigma(z)}} du \exp(u^2)(1 + \mathrm{erf}(u)) \right)^{-1}. \tag{A.64}$$

The two first moments of the distribution of frequencies can then be determined in a self-consistent way, using

$$\overline{v}_0 = \int dz\rho(z)v_0(z), \quad \overline{v_0^2} = \int dz\rho(z)v_0^2(z).$$

These equations, together with equations A.62–A.64, fully determine the whole distribution of stationary frequencies, which can be obtained using the relation

$$P(v) = \int dz\rho(z)\delta(v - v_0(z)).$$

A.5.2 Linear Stability Analysis. The linear stability analysis of section A.1 can be generalized to the inhomogeneous network. We give here the main steps of this analysis.

We expand the frequencies around the stationary frequency,

$$\nu(z) = \nu_0(z)\left(1 + n_1(z, t) + \cdots\right),$$

and, defining for each z $y = (x - \mu_0(z))/\sigma_0(z)$,

$$P = \frac{2\tau\nu_0(z)}{\sigma_0(z)}(Q_0(y, z) + Q_1(y, z, t) + \cdots).$$

The moments of the spatial distribution of frequencies can be expanded in the same way:

$$\overline{\nu} = \overline{\nu}_0\left(1 + \overline{n}_1(t) + \cdots\right),$$

$$\overline{\nu^2} = \overline{\nu_0^2}\left(1 + \overline{n_1^2}(t) + \cdots\right),$$

where

$$\overline{n}_1(t) = \frac{1}{\overline{\nu}_0}\int dz\rho(z)\nu_0(z)n_1(z, t)$$

$$\overline{n_1^2}(t) = \frac{2}{\overline{\nu_0^2}}\int dz\rho(z)\nu_0^2(z)n_1(z, t).$$

The Fokker-Planck equation at first order is

$$\tau\frac{\partial Q_1}{\partial t} = \mathcal{L}[Q_1] + \frac{\left(H_1(z)\overline{n}_1(t - \delta) + H_2(z)\overline{n_1^2}(t - \delta)\right)}{2}\frac{\partial^2 Q_1}{\partial y^2}$$

$$+ \left(G_1(z)\overline{n}_1(t - \delta) + G_2(z)\overline{n_1^2}(t - \delta)\right)\frac{\partial Q_1}{\partial y} \qquad (A.65)$$

where

$$G_1(z) = \frac{JC\overline{\nu}_0\tau - \epsilon J\tau z\sqrt{C\left(\overline{\nu_0^2} - \epsilon\overline{\nu}_0^2\right)}\frac{\overline{\nu_0^2}}{\overline{\nu_0^2} - \epsilon\overline{\nu}_0^2}}{\sigma_0(z)}$$

$$G_2(z) = \frac{J\tau z\sqrt{C\left(\overline{\nu_0^2} - \epsilon\overline{\nu}_0^2\right)}\frac{\overline{\nu_0^2}}{\overline{\nu_0^2} - \epsilon\overline{\nu}_0^2}}{2\sigma_0(z)}$$

$$H_1(z) = \frac{J^2C\overline{\nu}_0\tau - \epsilon J^2\tau z\sqrt{C\left(\overline{\nu_0^2} - \epsilon\overline{\nu}_0^2\right)}\frac{\overline{\nu_0^2}}{\overline{\nu_0^2} - \epsilon\overline{\nu}_0^2}}{\sigma_0^2(z)}$$

$$H_2(z) = \frac{J^2 \tau z \sqrt{C\left(\overline{v_0^2} - \epsilon \overline{v}_0^2\right)} \frac{\overline{v_0^2}}{\overline{v_0^2} - \epsilon \overline{v}_0^2}}{2\sigma_0^2(z)}.$$

The eigenmodes of equation A.65 can be written

$$Q_1(y, z, t) = \hat{Q}_1(y, z) \exp(i\omega t/\tau) + \text{c.c.}$$

$$n_1(z, t) = \hat{n}_1(z) \exp(i\omega t/\tau) + \text{c.c.},$$

leading to the solvability conditions, for each z,

$$\hat{n}_1(z) = I(z)\overline{\hat{n}_1} + J(z)\overline{\hat{n}_1^2},$$

where

$$I(z) = \frac{\tilde{W}_2\left[R_1\right](y_\theta) - \left[\tilde{W}_2\left[R_1\right](y)\right]_{y_r^-}^{y_r^+} + H_1(z)e^{-i\omega\delta/\tau}\left(\tilde{\phi}_2(y_\theta) - \tilde{\phi}_2(y_r)\right)}{\tilde{\phi}_2(y_\theta) - \tilde{\phi}_2(y_r)}$$

$$J(z) = \frac{\tilde{W}_2\left[R_2\right](y_\theta) - \left[\tilde{W}_2\left[R_2\right](y)\right]_{y_r^-}^{y_r^+} + H_2(z)e^{-i\omega\delta/\tau}\left(\tilde{\phi}_2(y_\theta) - \tilde{\phi}_2(y_r)\right)}{\tilde{\phi}_2(y_\theta) - \tilde{\phi}_2(y_r)}$$

with

$$R_{1,2} = e^{-i\omega\delta/\tau}\left(\frac{G_{1,2}(z)}{1 + iw}\frac{dQ_0(y)}{dy} + \frac{H_{1,2}(z)}{2(2 + iw)}\frac{d^2Q_0(y)}{dy^2}\right). \tag{A.66}$$

Multiplying the above equation by ρv_0 ($2\rho v_0^2$) and integrating with respect to z, we obtain

$$\overline{\hat{n}_1} = \frac{\langle v_0 I\rangle}{\overline{v_0}}\overline{\hat{n}_1} + \frac{\langle v_0 J\rangle}{\overline{v_0}}\overline{\hat{n}_1^2}$$

$$\overline{\hat{n}_1^2} = 2\frac{\langle v_0^2 I\rangle}{\overline{v_0^2}}\overline{\hat{n}_1} + 2\frac{\langle v_0^2 J\rangle}{\overline{v_0^2}}\overline{\hat{n}_1^2},$$

where we use the notation $\langle\cdots\rangle = \int dz\rho(z)\dots$ The instability point together with the associated frequency are given by the condition that the associated determinant vanishes, that is,

$$1 = \frac{\langle v_0 I\rangle}{\overline{v_0}} + 2\frac{\langle v_0^2 J\rangle}{\overline{v_0^2}} + 2\frac{\langle v_0^2 I\rangle\langle v_0 J\rangle - \langle v_0^2 J\rangle\langle v_0 I\rangle}{\overline{v_0}\,\overline{v_0^2}}.$$

The relative degree of synchrony of population z with the collective oscillation is given by

$$\hat{n}_1(z) = \overline{\hat{n}_1}\left(I(z) + J(z)\frac{2\frac{\langle v_0^2 I\rangle}{\overline{v_0^2}}}{\left(1 - 2\frac{\langle v_0^2 J\rangle}{\overline{v_0^2}}\right)}\right).$$

References

Abbott, L. F., & van Vreeswijk, C. (1993). Asynchronous states in a network of pulse-coupled oscillators. *Phys. Rev. E, 48*, 1483.

Abeles, M. (1991). *Corticonics*. New York: Cambridge University Press.

Abramowitz, M., & Stegun, I. A. (1970). *Tables of mathematical functions*. New York: Dover.

Amit, D. J., & Brunel, N. (1997a). A model of global spontaneous activity and local delay activity during delay periods in the cerebral cortex. *Cerebral Cortex, 7*, 237.

Amit, D. J., & Brunel, N. (1997b). Dynamics of recurrent networks of spiking neurons before and after learning. *Network, 8*, 373.

Bragin, A., Jando, G., Nadasdy, Z., Hetke, J., Wise, K., & Buzsáki, G. (1995). Gamma (40–100 Hz) oscillation in the hippocampus of the behaving rat. *J. Neurosci., 15*, 47.

Braitenberg, V., & Schütz, A. (1991). *Anatomy of cortex*. Berlin: Springer-Verlag.

Bender, C. M., & Orszag, S. A. (1987). *Advanced mathematical methods for scientists and engineers*. New York: McGraw-Hill.

Buzsáki, G., & Chrobak, J. J. (1995). Temporal structure in spatially organized neuronal ensembles: A role for interneuronal networks. *Current Opinion in Neurobiology, 5*, 504.

Buzsáki, G., Horvath, Z., Urioste, R., Hetke, J., & Wise, K. (1992). High frequency network oscillation in the hippocampus. *Science, 256*, 1025.

Chandrasekhar, S. (1943). Stochastic problems in physics and astronomy. *Rev. Mod. Phys., 15*, 1.

Csicsvari, J., Hirase, H., Czurko, A., & Buzsáki, G. (1998). Reliability and state dependence of pyramidal cell-interneuron synapses in the hippocampus: An ensemble approach in the behaving rat. *Neuron, 21*, 179–189.

Delaney, K. R., Gelperin, A., Fee, M. S., Flores, J. A., Gervais, R., Tank, D. W., & Kleinfeld, D. (1994). Waves and stimulus-modulated dynamics in an oscillating olfactory network. *Proc. Natl. Acad. Sci. USA, 91*, 669–673.

Eckhorn, R., Frien, A., Bauer, R., Woelbern, T., & Kehr, H. (1993). High frequency (60–90 Hz) oscillations in primary visual cortex of awake monkey. *NeuroReport, 4*, 243–246.

Fisahn, A., Pike, F. G., Buhl, E. H., & Paulsen, O. (1998). Cholinergic induction of network oscillations at 40hz in the hippocampus *in vitro*. *Nature, 394*, 186–189.

Gardiner, C. W. (1983). *Handbook of stochastic methods*. Berlin: Springer-Verlag.

Gerstner, W. (1995). Time structure of the activity in neural network models. *Phys. Rev. E, 51*, 738–758.

Gerstner, W., van Hemmen, J. L., & Cowan, J. D. (1996). What matters in neuronal locking? *Neural Computation, 8*, 1653–1676.

Golomb, D., & Rinzel, J. (1994). Clustering in globally coupled inhibitory neurons. *Physica D, 72*, 259–282.

Gray, C. M. (1994). Synchronous oscillations in neuronal systems: Mechanisms and functions. *J. Comput. Neurosci., 1*, 11–38.

Gray, C. M., König, P., Engel, A. K., & Singer, W. (1989). Oscillatory responses in cat visual cortex exhibit inter-columnar synchronization which reflects global stimulus patterns. *Nature, 338*, 334.

Gray, C. M., & McCormick, D. A. (1996). Chattering cells: Superficial pyramidal neurons contributing to the generation of synchronous oscillations in the visual cortex. *Science, 274*, 109.

Hansel, D., Mato, G., & Meunier, C. (1995). Synchrony in excitatory neural networks. *Neural Computation, 7*, 307.

Hirsch, M. W., & Smale, S. (1974). *Differential equations, dynamical systems and linear algebra*. New York: Academic Press.

Kopell, N., & LeMasson, G. (1994). Rhythmogenesis, amplitude modulation, and multiplexing in a cortical architecture. *Proc. Natl. Acad. Sci. USA, 91*, 10586–10590.

Kreiter, A. K., & Singer, W. (1996). Stimulus-dependent synchronization of neuronal responses in the visual cortex of the awake macaque monkey. *J. Neurosci., 16*, 2381.

Laurent, G., & Davidowitz, H. (1994). Encoding of olfactory information with oscillating neural assemblies, *Science, 265*, 1872.

MacLeod, K. and Laurent, G. (1996). Distinct mechanisms for synchronization and temporal patterning of odor-encoding neural assemblies. *Science, 274*, 976–979.

Mirollo, R. E., & Strogatz, S. H. (1990). Synchronization of pulse-coupled biological oscillators. *SIAM J. Appl. Math., 50*, 1645.

Prechtl, J. C., Cohen, L. B., Pesaran, B., Mitra, P. P., & Kleinfeld, D. (1997). Visual stimuli induce waves of electrical activity in turtle cortex. *Proc. Natl. Acad. Sci. USA, 94*, 7621–7626.

Rappel, W. J., & Karma, A. (1996). Noise-induced coherence in neural networks. *Phys. Rev. Lett., 77*, 3256–3259.

Ritz, R., & Sejnowski, T. J. (1997). Synchronous oscillatory activity in sensory systems: New vistas on mechanisms. *Current Opinion in Neurobiology, 7*, 536–546.

Sakaguchi, H., Shinomoto, S., & Kuramoto, Y. (1988). Phase transitions and their bifurcation analysis in a large population of active rotators with mean-field coupling. *Prog. Theor. Phys., 79*, 600–607.

Singer, W., & Gray, C. M. (1995). Visual feature integration and the temporal correlation hypothesis. *Ann. Rev. Neurosci., 18*, 555.

Stopfer, M., Bhagavan, S., Smith, B. H., & Laurent, G. (1997). Impaired odour discrimination on desynchronization of odour-encoding neural assemblies. *Nature, 390*, 70–74.

Strogatz, S. H., & Mirollo, R. E. (1991). Stability of incoherence in a population of coupled oscillators. *J. Stat. Phys., 63*, 613–635.

Traub, R. D., Miles, R., & Wong, R. K. S. (1989). Model of the origin of rhythmic population oscillations in the hippocampal slice. *Science, 243*, 1319.

Traub, R. D., Whittington, M. A., Colling, S. B., Buzsáki, G., & Jefferys, J. G. R. (1996). Analysis of gamma rhythms in the rat hippocampus *in vitro* and *in vivo*. *J. Physiol., 493*, 471.

Treves, A. (1993). Mean-field analysis of neuronal spike dynamics. *Network, 4*, 259–284.

Tsodyks, M., & Sejnowski, T. (1995). Rapid state switching in balanced cortical network models. *Network, 6*, 111–124.

van Vreeswijk, C. (1996). Partial synchronization in populations of pulse-coupled oscillators. *Phys. Rev. E, 54*, 5522–5537.

van Vreeswijk, C., Abbott, L., & Ermentrout, G. B. (1994). When inhibition not excitation synchronizes neural firing. *J. Comput. Neurosci., 1*, 313.

van Vreeswijk, C., & Sompolinsky, H. (1996). Chaos in neuronal networks with balanced excitatory and inhibitory activity. *Science, 274*, 1724–1726.

Wang, X-J., & Buzsáki, G. (1996). Gamma oscillation by synaptic inhibition in a hippocampal interneuronal network model. *J. Neurosci., 16*, 6402.

Wang, X-J., Golomb, D., & Rinzel, J. (1995). Emergent spindle oscillations and intermittent burst firing in a thalamic model: Specific neuronal mechanisms. *Proc. Natl. Acad. Sci. USA, 92*, 5577–5581.

Whittington, M. A., Traub, R. D., & Jefferys, J. G. R. (1995). Synchronized oscillations in interneuron networks driven by metabotropic glutamate receptor activation. *Nature, 373*, 612.

Ylinen, A., Bragin, A., Nadasdy, Z., Jando, G., Szabo, I., Sik, A., & Buzsáki, G. (1995). Sharp-wave associated high frequency oscillation (200 Hz) in the intact hippocampus: Network and intracellular mechanisms. *J. Neurosci., 15*, 30.